Final report

Geometry- and load-specific optimization of the collagen network's fibre orientation in the lumbar spine's annulus fibrosus

Author:
Andreas Schmocker

Supervisors:
Dr. Jerome Noally
Dr. Damien Lacroix
Dr. Dominique Pioletti

January 22, 2010

Contents

1 Abstract

In Europe, low back pain (LBP) affects the quality of life of up to 30% of the active population. Although the origin of LBP is not well identified and is probably not unique, epidemiological studies suggest that the severity of the disease is correlated with mechanical factors. The lumbar spine is a complex structure where bone, cartilage, ligaments, and muscles have specific and functional mechanical interactions that depend on the shape and structure of each tissue. Thus, any local tissue abnormality may generate non-physiological loadings on surrounding tissues, extending or catalysing a pre-existing degenerative process. To date, lumbar spine finite element modelling is one of the most promising methods to thoroughly investigate functional load transfers between the different spine tissues. However, many geometrical or mechanical parameters used for tissue modelling are still not quantified and need to be assumed.

Previous computational studies demonstrated that the intervertebral disc (IVD) plays a key role in distributing the internal forces across the lumbar spine structure. Within the IVD, together with the nucleus pulposus (NP) pressure, the annulus fibrosus (AF) collagen organization is one of the most influential parameter for the disc stabilization. However, AF collagen organization is not unique and seems to depend on the particularity of spine morphologies. Therefore, any lumbar spine model based on particular geometrical data would require specific definitions of fibre-induced AF anisotropy. Unfortunately, particular AF anisotropies are hardly measurable. Thus, the present project aims to investigate the stabilization of a L4-L5

lumbar spine bi-segment finite element model as a function of the AF fibre orientations. For this, a mathematical function, based on local AF matrix shear strains, fibre stresses and fibre stress distribution has been proposed. In this function was implemented and was partially validated on smaller AF model. Enhancements could be proposed and be applied to the L4-L5 model. Methods and procedure to optimize annulus AF orientations could be validated. The proposed evaluation function had to be changed. It was found that an optimal orientation depends mainly on fibre stress and matrix shear stress. The optimizations converged to average angles between 32 and 68 and radial gradients between 10 and 17 degree. Tangential gradients could not be found. Moreover a critical fibre angle could be determined where fibre under uni-axial load are not loaded any more.

Using literature data it was possible to solve one of the main issues of collagen fibre orientations in the AF and to bring together the two hypothesis of either a only radial or only a tangential gradient.

Moreover it was concluded that pre-stress respectively hoop stress is an non-negligible factor which has to be accounted for in IVD finite element models.

2 Introduction

This report resumes the work which was done during the Master thesis of Andreas Schmocker at the Institute for Bioengineering of Catalunya (IBEC). It was supervised by Jérôme Noailly and Damien Lacroix (IBEC) and tutorized by Dominique Pioletti from the Swiss Federal Institute of Technology

(EPFL).

On one hand it shall illustrate the scientific findings of the of the last four months and on the other hand it is dedicated to any person continuing the project or the research line.

The introduction has a top-down structure, starting with low back pain, the final reason of our research, then introducing anatomical and structural issues, getting more and more specific within the state of the art.

2.1 Low back pain

According to the European Agency for health and safety at work almost 30% of the population has low back pain sometime. Men and women are equally affected. It occurs most often between ages 30 and 50, due in part to the aging process but also as a result of sedentary life styles with too little (sometimes punctuated by too much) exercise. The risk of experiencing low back pain from disc disease or spinal degeneration increases with age. To counter low back pain various therapeutic modalities have been attempted with minimal long-term success to alleviate the poorly described disc-related pain[1].

Yet, heavy loading conditions and high flexibility make the human lumbar spine to be quite sensitive to daily poor ergonomic factors and convert it into a preferential site for mechanically induced traumas and degenerations [2]. There is no single cause for low back pain. The following conditions could be related to it [3]:

(a) Bulging disc

(b) Cauda equina syndrome

(c) Spinal stenosis

(d) Skeletal irregularities

(e) Fibromyalgia

(f) Spondylolystois

Although low back pain has always affected human beings, it has turned into one of the major healthcare problem of the industrialized countries [2]. 30% of European workers suffer from back pain and between 60% and 90% of people will undergo low back disorders at some point in their life [4].
According to [5], in Belgium, 29% of the total number of sick-leave days are attributable to low back pain which corresponds to a total economic loss of 992.6 million Euros or 5.7 million days of absenteeism per year. In the United Kingdom, back pain was identified as the most common cause of disability in young adults with a 100 million labour days lost each year. In Sweden in 1987 a total number 28 million days lost was reported [6]. Extrapolating the data from Belgium and assuming a population of one billion (for the US and Europe without Russia) the total economic cost in the western world could be roughly estimated around 100 billion Euros a year.

2.2 The human spine

The main function of the spine is to transfer external loads through the body. It also ensure controlled flexibility between head, trunk and pelvis

and the protection of the spinal nerve roots from loads, shocks and excessive displacement [7, 8]. The human spine consists of 33 or 34 vertebra and 23 intervertebral discs (IVD), and is atomically divided into five subsections (Fig. 1), listed from the head to the pelvis:

(a) Cervical spine (C1-7)

(b) Thoracic spine (T1-12)

(c) Lumbar spine (L1-5)

(d) Sacrum (S1-5)

(e) Coccyx

Each subsection is characterized by its own vertebra morphology, which is correlated with the required flexibility or resistance to the transferred loads. Except the for sacrum, the coccyx and the first two cervical vertebra a IVD is sandwiched between all vertebra.

2.3 Lumbar spine

2.3.1 Anatomy

The anterior and main part of a vertebra, the vertebral body, consists of trabecular bone which is surrounded laterally by a cortical shell and by the bony endplates, at the higher and lower end. The vertebral bodies bear the main loads the lumbar spine is exposed to. The posterior parts, the pedicle, lamina and the processes (Fig. 2) contribute to block extensive rotations

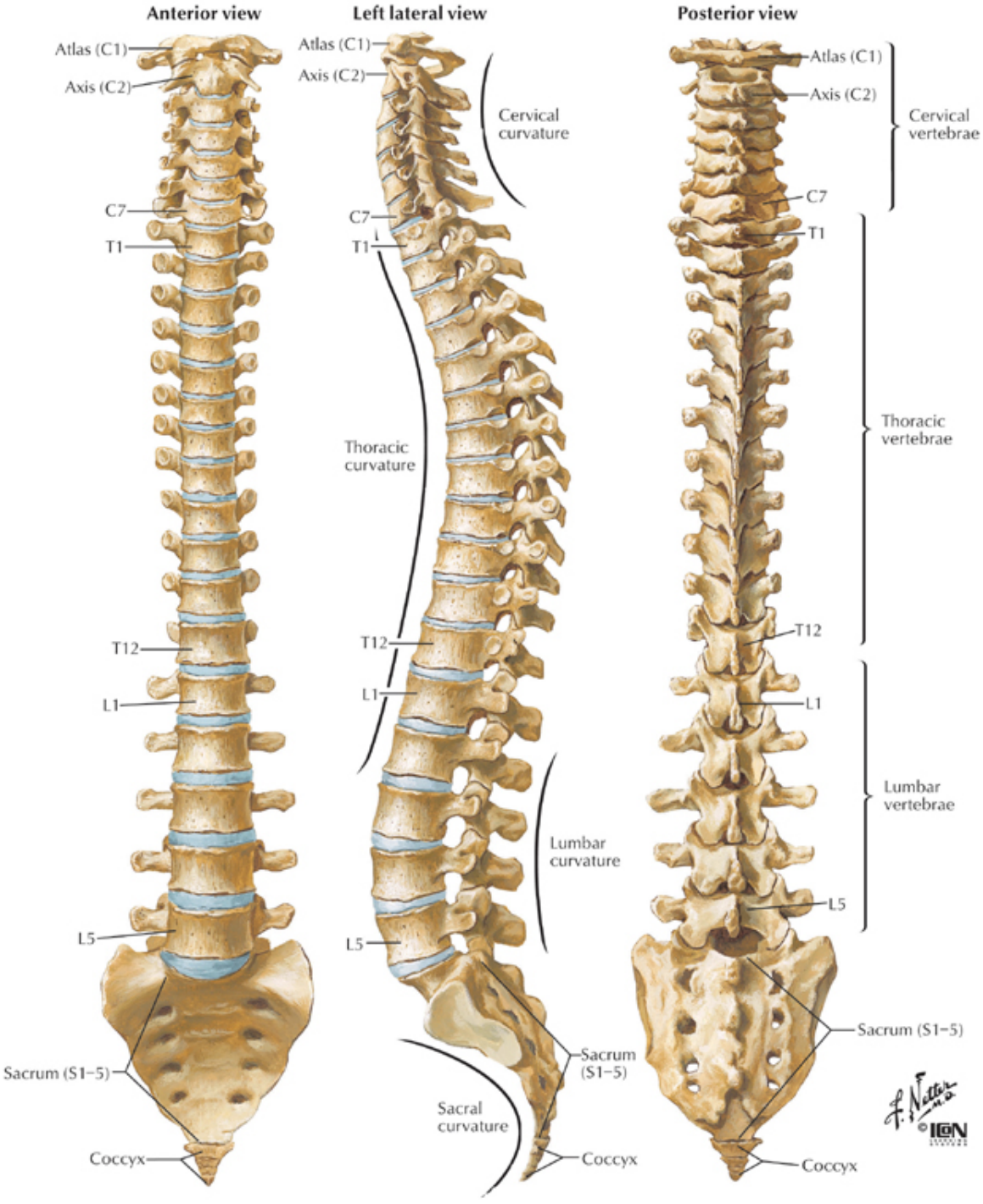

Figure 1. The spine, schematic view of the osseous lumbar spine, including vertebral discs [9].

around the three anatomical axis and protect the spinal nerve roots.

With heights of 8 to 10 cm, the lumbar IVDs account for 30% - 35% of the total lumbar spine height. With an average diameter around 4 cm, the lumbar IVD surface transversal cross-section is bigger than that of the other IVDs. They provide flexibility and absorb and transmit loads. Therefore, the lumbar discs consist of a specialized structure, particularly able to resist compressive loads, while enabling the mechanically complex movements required between the trunk and the pelvis. The nucleus pulposus (NP) in the center is surrounded by the annulus fibrosus (AF) laterally and by the cartilaginous endplates at the bottom and top ends (Fig. 2).

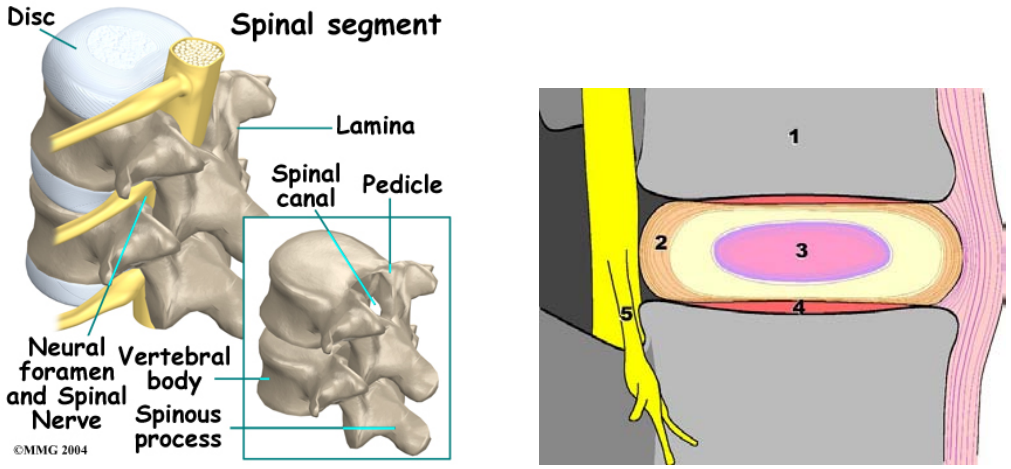

(a) (b)

Figure 2. Vertebra body and annulus fibrosus a) Two spinal segments with its major components [10] b) vertebral body(1), annulus fibrosus (2), nucleus pulposus (3), cartilagous endplantes (4) and spinal nerve root(5)[1].

2.3.2 Load transfer between the vertebra and IVD

The U.S. Consumer Product Safety Commission estimates that more than 13,260 injuries related to backpacks were treated at doctor's offices, clinics, and emergency rooms in the year 2000 [3].

Due to their position and as a consequence of muscle forces, the vertebrae and IVD in the lumbar spine have to resist to higher loadings than in other spine sections.

Compared to the IVD tissues, the vertebrae are much stiffer. However, the compressive loadings transmitted by the vertebra can be efficently bore by the IVD through a coordinated action between the nucleus pulposus and the annulus fibrosus. When compressed between the vertebral endplates, the soft and gel-like nucleus will is pressurized and extends laterally, which stresses the AF fibres. In other words, as the spine is loaded in compression or bending (the primary loading modes of the spine), tensile loads are transmitted to the well-organized, lamellar collagen fibre structure of the annulus fibrosus. Compression of the intervertebral disc results in outward bulging of the annulus fibrosus and fibre strains in the order of 3% [11].

2.3.3 Importance of the AF and its structure

Within each AF region, collagen bundles are distributed into concentric layers characterized by preferential fibre orientations [12, 13]. Typically collagen fibres have no compressive stiffness but provide most of the AF mechanical strength, as they can locally reorient and stretch [14] to resist tissue tractions and/or AF bulging when the disc is under compression. Anchored to

the top and bottom vertebrae, AF collagen bundles can also stretch as a response of IVD shear deformations. Thus, they play a key role in mechanically reinforcing the IVD and transmitting loads to other spine tissues under any kind of mechanical loading. However, since before stretching AF fibres need to align with the local loads felt by the annulus, IVD reinforcement and load transmissions should partly depend on undeformed fibre orientations. Accordingly several groups showed that AF and IVD mechanical properties depend strongly of fiber angle values [15–18]. Moreover it was reported that degeneration had a significant effect on fibre reorientation, which probably contributes to the mechanical disfunctioning of the degenerated disc. Therefore characterizing fibre initial orientation and reorientation in the human AF is important in order to fully understand and accurately model the relationship between IVD structure and function, and design functional tissue-engineered intervertebral discs [19].

2.4 State of the art

2.4.1 AF Anatomical description

The human lumbar AF is made out of 15 to 25 concentric collagen fibre [12] layers laterally wrapping the nucleus pulposus. The fibre orientation alternates from positive to negative from one layer to the next and forms a criss-cross pattern with altering fiber angle (fig. 5 and 3). Fibres consist out of collagen type I and II with collagen ratios[1] changing from layer to layer. The highest collagen I ratio is found in the outer AF decreasing gradually to

[1]Collagen I is stiffer than collagen II.

the inner AF. In total the collagen content rises up to 60% of the dry weight [20].

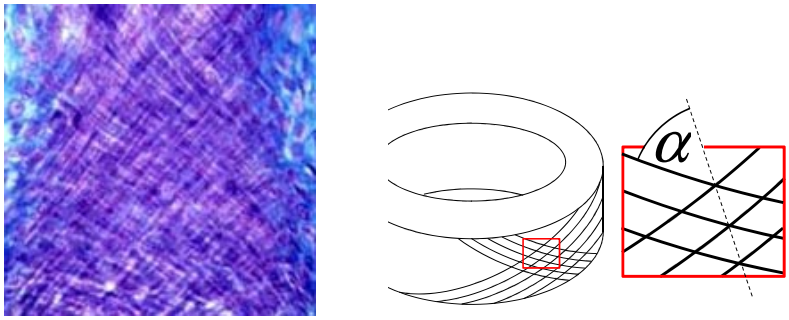

(a) (b)

Figure 3. a) Oriented cells of the embryonic annulus fibrosus [21] - collagen bundles are orientated in a criss-cross pattern. b) Global fibre angle constitution in the AF and definition of the fibre angle α.

In the literature several different fibre orientations exist:

(a) Constant fibre orientation of 30 ° in all AF layers and tangential segments (anterior, posterior, etc.) [12, 22]

(b) Fibre angles increase form 28 ° in the outer to 45 ° in the inner AF, no tangential change [23]

(c) No change in radial direction (through the tissue thickness), fibre angles change form 23.5 ° in the posterior to 67.3 ° in the anterior AF[24]

(d) Fibre angle decrease from the outer to the inner AF except for the posterior section. Tangentially maximal fibre angles (∼10 °;outer to ∼0 °;inner) were found in the posterior part and minimal fibre angles (33-57 °;outer and 65-70 °;inner) in the right anterior-lateral section [25].

Measurement b) and c) are schematically represented in (Fig. 4). These qualitative differences in AF fibre criss-cross pattern angle distributions lead to the question whether specific local angles maintain a functional relationship with local loadings and/or geometrical characteristics.

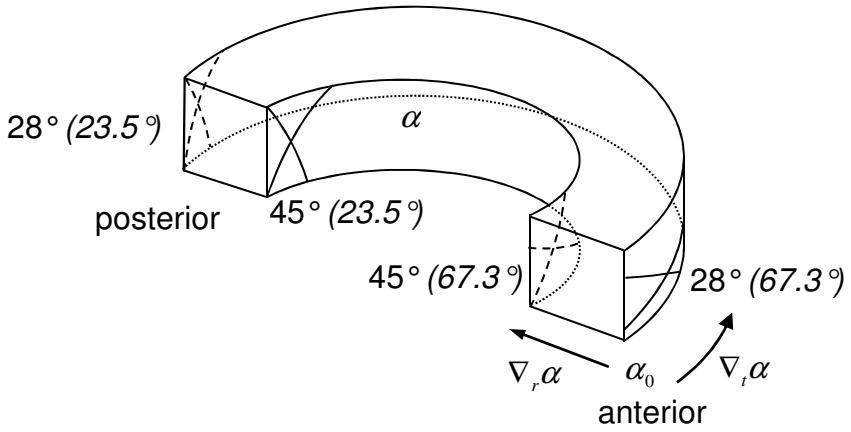

Figure 4. Representation of a semi annulus fibrosus. The criss-cross pattern changes from outer to inner AF and form anterior to posterior. The given angles present measurements (b): a radial gradient $\nabla_r\alpha$ of $+17°$ [23] and *(measurement (c): a tangential gradient of -43.8°)* [24].

2.4.2 Evaluation of collagen fibre orientations in soft connective tissues

i) Aorta and articular cartilage

An important topic in tissue engineering is remodelling. Several groups tried to model remodelling collagen fibre orientations in soft connective tissues, especially the aorta, aortic valves and different cartilages. Driessen proposed two algorithms based on the following hypothesises [26–28]:

(a) Collagen fibres align in the (positive) principal strain directions, respectively the directions of the eigenvectors with a positive eigenvalue.

(b) Collagen fibres align between the principal positive strain directions according to equation 1. The e_p being the preferred fibre direction.

$$\vec{e_{p,i}} = \frac{g_1\vec{e_1} \pm g_2\vec{e_2}}{\sqrt{g_1^2 + g_2^2}} \tag{1}$$

Where g_i:

$$g_j = \begin{cases} \varepsilon_j & \text{if } \varepsilon_j > 0 \\ 0 & \text{if } \varepsilon_j < 0 \end{cases} \tag{2}$$

ε_j being the eigenvalue corresponding to the eigenvector $\vec{e_j}$. In the case of one positive principal strain direction (i=1), one preferred fibre direction $\vec{e_{p,1}}$ is predicted. In case of two positive principal strain direction (i=1,2), two preferred fibre directions $\vec{e_{p,1}}, \vec{e_{p,1}}$ are predicted.

Remodeling analysis based on hypothesis a) could not reproduce the helical collagen orientation found in arteries. In articular cartilage the remodelling rule of hypothesis b) correctly predicted the collagen architecture, while hypothesis a) failed [28].

Moreover, Hariton et al. [29] suggested that collagen fibres align between the two highest principal stress directions similar as in Equations (1) and (2), but e_i being two eigenvectors attributed to the two highest positive stress eigenvalues, and ε_j being replace by those eigenvalues [29]. The hypothesis was able to model the collagen structure in the arterial wall and to minimize local shear stress and strain.

ii) Annulus fibrosus

In the IVD Noailly et al.[30] proposed a new type of collagen orientation evaluation function for the AF. This function takes into account fibre stress magnitude, fibre stress distribution and strain in the ground substance respectively the cells around the collagen fibres. Results were promising, since the proposed function was able to quantitatively relate the local AF loading to the studied local AF fibre orientations. A further evaluation of this function in terms of optimal fibre orientation prediction will be the main subject of this work and is precisely described in section 3.1.

2.5 Objectives of the project

As demonstrated previously, in most connective soft tissues, primary fibre orientations are correlated to mechanical loadings. In tissues like arteries, tendons, or ligaments, load patterns are sufficiently simple and repetitive so that maximum principal strain directions correspond to the alignment of the reinforcing fibres [31]. However, in fibrous tissues resisting to complex loads, the relation between primary fibre orientation and external loadings is not straightforward.

For lumbar spine AF's, different orientations in the literature suggest that fibre alignments are dependent on individual morphologies and physical activities. Thus, to explore the fibre-related stabilization of such tissues, a quantitative relationship between local fibre and tissue loadings was established, assuming that optimally oriented fibres should bear as much load as

possible, while limiting load concentrations and shear deformations within the tissue. The potential of such hypothesis to give rational fibre orientations will be tested through an optimization procedure. Thus, the aim of this master thesis is to evaluate a newly proposed objective function for AF fibre orientation, if necessary propose improvements and finally apply the algorithm to a complete lumbar spine L4-L5 segment finite element (FE) model, in function of different loads.

3 Materials and methods

In this section, the lumbar spine segment FE model and the fibre orientation optimization procedure will be introduced. Moreover, the validation process and runtime respectively convergence improvements are presented at the end of the section.

3.1 Evaluation function

In this study, the ”evaluation function”, ”objective” or ”fitness function” is a function attributing to a simulation output (e.g. displacement, strain, stress etc.) a normalized positive value that is a measurement or an evaluation of the current (simulated) fibre distribution. This objective function, the fibre contribution quality (FCQ)[30], will be used at every optimization step. It was constructed from the hypothesises that an optimal AF fibre criss-cross angle distribution shall:

(a) Maximize fibre stresses

(b) Counterbalance non-uniform fibre stress distributions trough the AF thickness

(c) Minimize matrix shear strains

Assumption a) was based on the mechanical fact that collagen fibres in soft connective tissues are the element providing the tissue with its main resistance. b) refers to the ability of fibres to avoid load concentrations , possible source of damage. This is based on an analogy with the hoop stress reduction in tick walled vessels [32]. c) refers to the ability of fibres to limit matrix shear strains, according to the functional role of layered structures, from an engineering point of view [33]. These hypothesises led to the following mathematical parameters:

(a) **Radial Mean Stress (RMS)**

$$RMS = \frac{\sum_{i=1}^{N_f} \sigma_{fibre,i}}{N_f} \tag{3}$$

σ_i being the stress in fibre i and N_f the total fibre number. RMS is zero when all fibres are unloaded and maximal when the fibres are aligned with the highest principal stress direction.

(b) **Radial Stress Distribution (RSD)**

$$RSD = \sum_{t=1}^{N_t=4} \sqrt{4a_t^2 + b_t^2} \tag{4}$$

where a and b are the coefficients of the first and second order degree terms of the fibre stress's quadratic regression over all fibres through

the AF thickness for one AF tangential quadrant i.e. anterior, lateral, posterio-lateral or posterior quadrant:

$$\sigma(\overline{r})_t = a_t\overline{r}^2 + b_t\overline{r} + c \tag{5}$$

Where t = anterior, lateral, posterio-lateral, posterior. RSD is zero in the case of a constant stress distribution and increases as fibre stress gradients appear through the AF thickness.

(c) **Matrix Shear Stress (MSE)**

$$MSE = \frac{\sum_{j=1}^{N_e} \varepsilon_{max,j} - \varepsilon_{min,j}}{2N_e} \tag{6}$$

$\varepsilon_{min,j}$ respectively $\varepsilon_{min,j}$ being minimal and maximal principal matrix strains at integration point j and N_e the total number of integration points. MSE is low in the case of mainly volumetric strains and increases with the degree of deviatoric deformation in the matrix.

The three parameters were normalized and scaled between zero and one (Eq. 7)

$$\overline{RMS} = \frac{RMS - RMS_{min}}{RMS_{max} - RMS_{min}} \tag{7a}$$

$$\overline{RSD} = \frac{RSD - RSD_{min}}{RSD_{max} - RSD_{min}} \tag{7b}$$

$$\overline{MSE} = \frac{MSE - MSE_{min}}{MSE_{max} - MSE_{min}} \tag{7c}$$

and integrated (Eq. 8) into one function, the Fibre Contribution Quality (FCQ) which was designed to reach a maximal value of one (optimal fibre

distribution) and minimal value of zero (worst fibre distribution).

$$\overline{FCQ} = \frac{\log(1 - e^{-2} + e^{\overline{RMS}-\overline{RSD}-\overline{MSE}})}{\log(1 + e^{1} - e^{-2})} \tag{8}$$

One important issue is how to define minimal and maximal values for parameter scaling and normalization (Eq. 7). First, six optimisations were run to find each of them. Yet, due to computation time but also to the position of minima and maxima, this was not a realistic option, especially for large FE models and was therefore aborted. Second option was to evaluate a limited number of fibre orientations, where maximal or minimal values were expected and then to adapt dynamically, if the algorithm encountered a lower or higher parameter value during the optimisation. However, this method was considered not to be deterministic enough, because it was sometimes difficult to say where a maximal and minimal parameter values occur. Thus, in the end fibre angles were changed between 0 and 90 degree for α, $\nabla_r\alpha$ and $\nabla_t\alpha$ using a step size of 10 °. Out of this different fibre orientations maxima and minima values were chosen and then during the optimization dynamically adapted if it was necessary.

Equations (3) to (7) are those used for the main simulations, but enhancements were done and presented in Section 4.2.2. Moreover a summary is given in table 4.

3.2 Finite element modelling (FEM)

To run the simulations, three different FE models, from a very simple to a complete L4-L5 segment model, were used. The used FE software was Marc

Mentat (MSC Software, Santa Ana, CA, USA). Non-linear fibre properties and mechanical behaviours were implemented using Fortran subroutines.

3.2.1 Fibre orientation in the finite element model

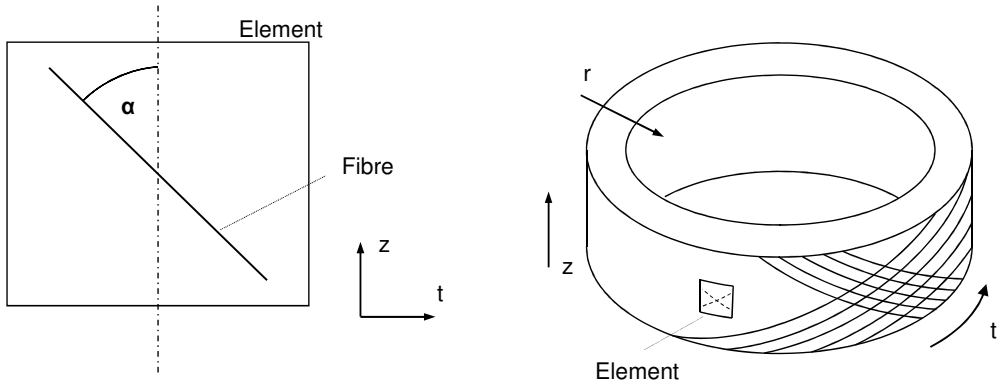

(a) (b)

Figure 5. a) The fibre angle α is the angle between the fibre and the vertical axis of the element (z). b) The fibre angle changes sign in direction of the AF thickness (r) from one fibre layer to the next. Finally two axes (r and t) were used to define the local fibre orientation of one element (Eq. 9).

Fibre orientations was defined with respect to the vertical element axis z as presented in figure 5. Moreover, the main assumption when implementing fibre orientations was that fibre angles vary linearly in radial (through AF tissue thickness - r axis and tangential direction (from anterior to posterior - t axis (Fig. 5). Thus, the function defining a local angle was chosen as follow:

$$\alpha(\overline{r},\overline{t}) = \alpha_0 + \nabla_r\alpha * \overline{r} + \nabla_t\alpha * \overline{t} \tag{9}$$

Where $\overline{r} = r/r_{max}$ and $\overline{t} = t/t_{max}$. Hence, $\overline{r}$ is zero in the outermost AF layer and one in the innermost. $\overline{t}$ is zero in the anterior and one in the pos-

terior AF. 5 has the advantage that maximal or minimal fibre angles can be calculated and visualized easily. For example if both gradient are positive the minimal angle is α_0 and the maximal angle $\alpha_0 + \nabla_r \alpha + \nabla_t \alpha$. An example of tangential and radial gradients is given in figure 4.

3.2.2 Geometries and boundary conditions

Because of the complexity of the loads transmitted to the AF, it can be very time-consuming to directly assess the FCQ objective function with the complete lumbar spine segment model. Therefore, different simple geometries were used first, which permitted to tackle a problem at different complexity levels. Moreover the use of several models allowed to do useful comparisons to evaluate, change and validate the FCQ function. The geometries presented in the report are (Fig. 6):

(a) A simple cuboid model mainly used to assess the basic behaviour of automatic fibre orientation and possible convergence problems.

(b) A computationally inexpensive semi-cylinder model, which permitted to run simulations with a simplified geometry close to the real AF. It consists of a semi ring and the NP was replaced by an constant pressure, internal to the ring .

(c) A complete L4-L5 lumbar spine segment model was used for the final validation of the FCQ function. It was adapted from a validated L3-L5 model [2].

In Table 1 all relevant geometrical and modelling information is summarized. The semi-cylinder and the complete model were symmetric in respect to the sagittal plane.

For the L4-L5 segment model, maximum load magnitudes leading to convergence were applied and being in the range of physiologically admissible loads for mono-segmental specimens [11]. For the small model a big issue was whether to choose constant loads or constant deformations. Finally it was considered that constant deformations were more realistic and easier to interpret.

3.2.3 Material properties

In general, the material properties of the simplified models were more or less the same as for the complete model. Collagen I content was homogenized by averaging values of the L4-L5 segment model. Implemented properties are presented in table 1 and as the L4-L5 model was adapted from [2] properties not related to the AF are not presented.

AF matrix was modelled using a hyper-elastic Mooney-Rivlin incompressible material. To model the AF fibres a collagen I-dependant hypo-elastic [2]approximation with a main linear and power law toe part was used [2]. Moreover the fibre stress is assumed to be zero under compression. The fibre stress implemented in Marc Mentat is $S = \frac{E}{2}(T^T : CT - 1)$ (linear case), where E and S are material strain and stress, C is fourth order elastic tensor and T texture tensor (orientation vector's vector direct product)[43].

[2]Acient Greek: *hypo*, "under"; *hyper*, "over". A hypo-elastic material law is a simplified non-linear elastic constitution model, behaves like a hyper-elastic model, but is not deduced form a strain energy function.

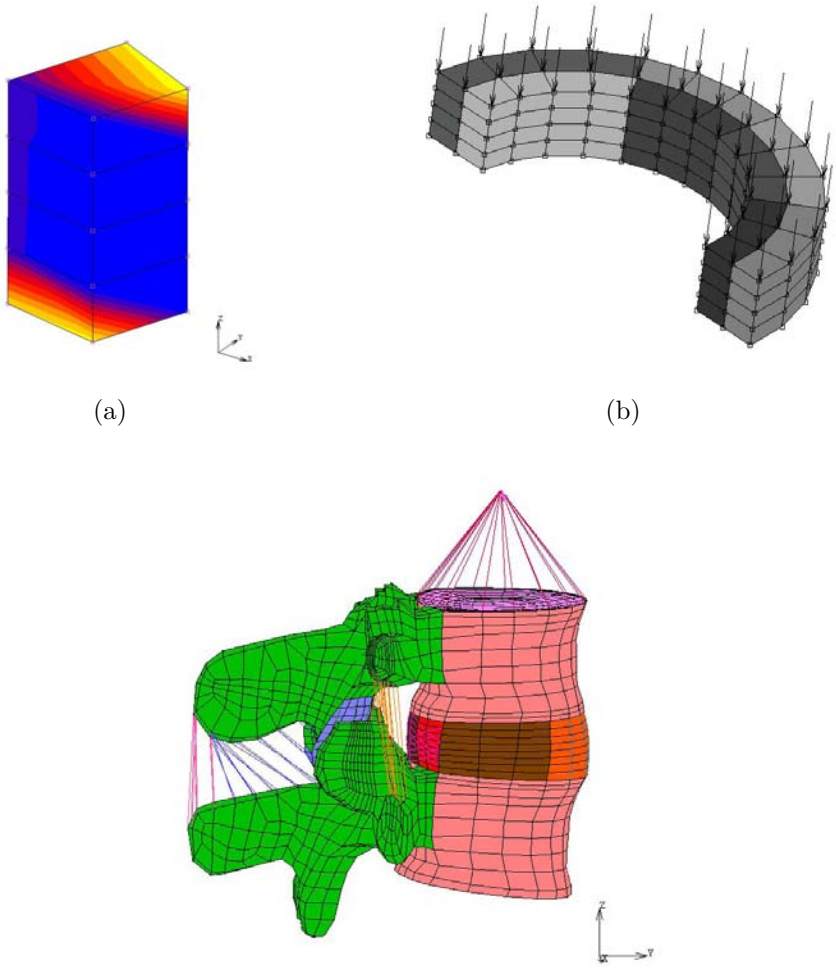

(a) (b)

(c)

Figure 6. Used geometries a): simple cuboid model b): semi-cylinder model c): complete L4-L5 lumbar spine segment model.

	simple cuboid	**semi-cylinder**	**L4-L5 model**
Geometry			
Number (#) of elements	16	208	8931
# of radial layers	5	10	20
# of tangential sections	1	4	4
Dimensions in elements (r,t,z)	(1,1,8)	(2,13,4)	(4,20,8)
AF element type	hex	hex	hex
Boundary conditions			
Fixed nodes	Base nodes (z=0) Upper nodes (z=10mm)	Base nodes (z=0) Upper nodes (z=10mm)	Three fist base nodes (L5)
Applied forces or strain	Axial* strain [± 10%]	Axial* strain [± 10%] internal radial pressure [0.15 MPa]	Flexion [6 Nm] Extension [10 Nm] Torsion [9 Nm] Compression [0.38 MPa]
Material properties			
AF matrix**	0.25 | 0 | 0 [44]	0.25 | 0 | 0 [44]	0.0595 | 0.0002 | 0.0296 (out) 0.053 | 0.001 | 0.058 (mid) 0.040 | 0.006 | 0.032 (in)
Collagen I content***	0.55 | 0.55 | 0.55 | 0.55	0.55 | 0.55 | 0.55 | 0.55	0.78 | 0.59 | 0.40 | 0.34

Table 1. Model specific properties: Geometry and boundary conditions. * Vertical axis z respectively vertical to the transverse plane. ** Mooney-Rivlin parameters: C_{10} | C_{01} | C_{11} of the energy function: $W = C_{10}(\overline{I}_1 - 3) + C_{01}(\overline{I}_2 - 3) + C_{11}(\overline{I}_1 - 3)(\overline{I}_2 - 3)$ where $\overline{I}_k$ are the invariant of the deviatoric part of the right Cauchy-Green tensor. Source L4-L5 model: [30]. *** outer AF | middle 1 | middle 2 | inner AF

3.2.4 Analysis

All forces or displacements were applied on a linear growing time scale which led to better convergence. Time steps were constant (total time steps between 30 and 1000), but allowing cutback. As convergence criteria relative force residuals (value 0.1) were implemented. Only implicit discretisation was used (mostly Single-step Houbolt, else Newmark). To master the non-linearity, total lagrangian large strain method was applied. All in Marc Mentat existing solvers were tested on the L4-L5 geometry, finally the mixed iterative-direct solver showed best performance (section 3.4) and was used.

3.3 Optimization of fibre orientation

Some parts in this section are purely technical (e.g. 3.3.2) and dedicated to people, who want to take over the project and develop it further.

As the main aim was to find the optimal fibre orientation an iterative optimization procedure was necessary. Thus, Matlab (MathWorks Inc.) was used to run FE software Marc Mentat, extract the data and run the optimization algorithm.

When talking about an iteration of the optimization algorithm, it is referred to as *optimization iteration* and when talking about one iteration of a FE simulation it is referred to as *simulation iteration*.

3.3.1 Algorithm

Usually to find the minimum or maximum of an objective function (in our case FCQ) a methods taking into account function and gradient value at a

specific point are used[3]. In our case no analytical function exists therefore a discrete method has to be used. Due to the time intensive objective function evaluation (one FE simulation) and the three dimensional solution space (α_0, $\nabla_r\alpha$ and $\nabla_t\alpha$) discrete search methods were chosen and more specific the version of the in Matlab implemented simplex algorithm. A simplex algorithm evaluates the function value at each point of the simplex (in 2D a triangle, in 3D a pyramid, etc.), compares the three, four or n+1 values, chooses the highest one (if the global minimum is of interest) or the lowest one (maximum) and replaces it with a new point, which is the creation of the next simplex or one optimization iteration. The advantage of a simplex algorithm is its ability to solve discontinuous problems.

Furthermore, the use of genetic algorithms (GA), was test, but, due to its necessity of intensive fitness (objective) function evaluation, quickly aborted. In Annex A.0.2 a sample solution can be found. Although the use of an GA would be too time-intensive, its use either with reduced population size or in parallel was always left open. One possibility would be the use of a GA with limited population and generation size which induces after certain number of generations a discrete algorithm. This solution is also implemented into Matlab. For more information about GA check [34, 37].

3.3.2 Task organization

The flow diagram in Figure 7 presents the structure of the fibre orientation optimization. Among the Matlab M-files, Run_file.m initiates the optimiza-

[3]Because direct search methods neither compute nor approximate derivatives, they are also described as "derivative-free" [35].

tion(s) and delivers to Opti_fmin.m the initial position, name of the simulation and other parameters which are specific to each optimization (e.g. the maximal allowed number of function evaluations). In the Opti_fmin.m file is all information specific to one type of simulation (e.g. geometrical information, number of layer to evaluate, subroutine name, Marc Mentat .dat-file name etc.). Moreover, it contains the optimization algorithm command line, generates the graphical outputs and keeps track of the optimization steps. The optimization algorithm calls the F_eval.m file. As a Marc Mentat simulation required easily an hour or more F_eval.m checks first whether a simulation with a given α_0,$\nabla_r\alpha$ and $\nabla_t\alpha$ was already run. If this was the case it read the information out of the existing file, else it saved the α_0,$\nabla_r\alpha$ and $\nabla_t\alpha$ into the COMMON_VAR file, initialised a Marc Mentat simulation and read the strain and stress tensors from simu_results_#.txt once the simulation was finished. Finally it had to return one objective function value to the optimization algorithm: F_eval.m communicated stress and strain tensors to FCQ_eval.m which contains the mathematical formulations of the objective function $\overline{FCQ}$ and calculated its value for each iteration of the optimisation.

To evaluate just one $\overline{FCQ}$ value for a defined fibre orientation, the F_eval.m file can also be called directly from Run_file.m or from the Matlab command window. The only value it requires is a row vector containing a fibre orientation ($[\alpha_0, \nabla_r\alpha, \nabla_t\alpha]$).

There are a several values which have to be communicated between the different files. Parameter which are huge in size (e.g. stress and stain tensors) were handled as function arguments. Most of the other parameters were externally stored in .mat-files. Therefore at the beginning, each .m-file loaded

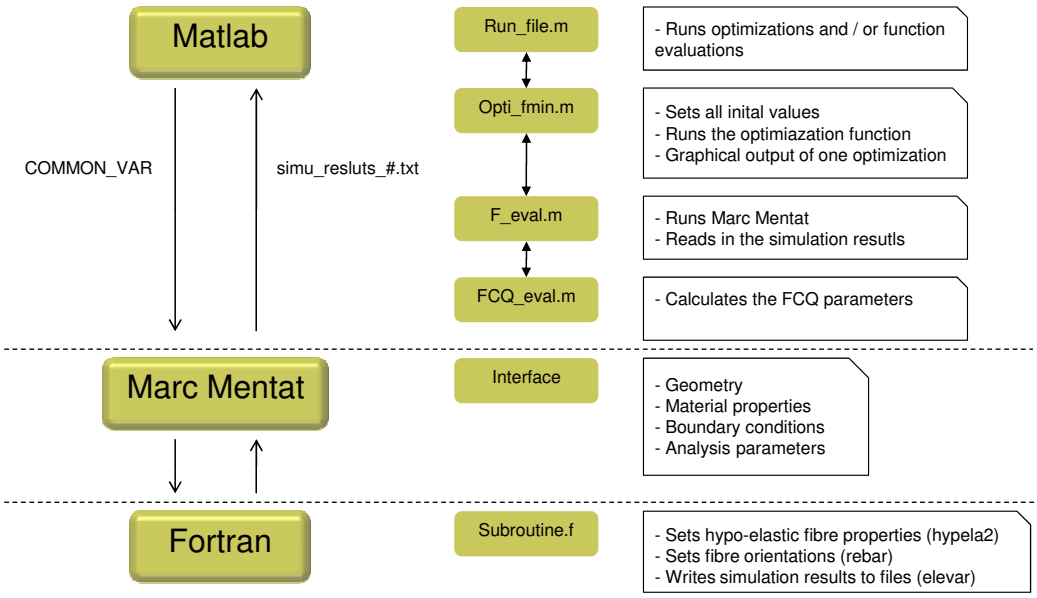

Figure 7. The flow diagram shows the optimization's main structure and gives an overview of each functional level.

the required parameters, which had been saved before by an other .m-file.

To keep track of several runs, an optimization or some iteratively performed fibre orientation evaluations two files were being written. The most important was iter_file.mat (generated by F_eval.m) and iter_FCQ.val.mat (generated by FCQ_eval.m). In both of them, one iteration was represented as one row. iter_file.mat tracks fibre angle data [°] (column 1 = α_0, 2 = $\nabla_r\alpha$, 3 = $\nabla_t\alpha$), $\overline{FCQ}$ function values (column 4) and required iteration time [s] (column 5). FCQ_eval.val.mat keeps track of $\overline{RMS}$ (column 1), $\overline{MSE}$ (column 2) and $\overline{RSD}$ (column 3) and of their absolute values (RMS,MSE,RSD = column 4-6). In column 7 again $\overline{FCQ}$ values, which allowed comparing values without changing the file.

The second operational level (Fig. 7) was Marc Mentat, where modelling pa-

rameters were introduced using the simulation interface. The lowest structural level is the Fortran subroutine file (e.g. subroutine_big_45.f) which was called by Marc Menatat for each simulation iteration. It contains three subroutines:

(a) Hypela2

(b) Rebar

(c) Elevar

According to the hypo-elastic material formulation, hypela2 attributes at each fibre and ligament strain level a corresponding tangent stiffness and stress value following predefined stress-strain curves [2]. There, collagen I volume fractions were defined.

rebar orientates the fibres and assigns to each rebar element a fibre vector. First, α_0,$\nabla_r\alpha$ and $\nabla_t\alpha$ are "read in" from the COMMON_VAR file (COMMON_VAR is included into the code as a common block, which helps significantly to reduce computational time). As the rebar subroutine had to return to Marc Mentat fibre vectors in global coordinates, the elements axes in the global system were calculated using the elements nodes coordinates, which served to define the three-dimensional rotation matrix.

In Marc Mentat each AF subsection (e.g. anterior/middle(1), post-lateral/outer etc.) was defined as a different material. Each material had a material number, which was used in the code to access subsection properties (fibre angles and collagen I content). Hence in the rebar subroutine a relative position consisting of $\bar{r}$ and $\bar{t}$ values were allocated. The same was done for the rebar

layers within each element. Finally using (Eq. 9) a fibre vector was defined, rotated using the rotation matrix and returned to Marc Mentat in global coordinates. In the L4-L5 model, the problem of wrong oriented elements was solved using a Euler rotation angles.

elevar writes the output files simu_results_#.txt. For each subsection or material, one file was written which permitted to further distinguish the fibre elements in Matlab. The files were written for one specific increment. This increment had to be the implemented in Marc Mentat.

For more information about the written code, see Sections C Fortran and B Matlab.

3.3.3 Error hunting and parameter overview

The aim of the chosen program(s) structure (Fig. 7)) is the ability to change geometry or mathematical models without modifying any basic code. Therefore, the amount of parameters is huge and code complexity could be source of a failure. Thus, it was decisive to implement a structure that permitted to quickly locate errors. The lowest level, where an error could occur was in the rebar subroutine (e.g. wrong n_r or n_t), the second lowest level was represented by parameters in Marc Mentat (solver, loads, etc.) and the third lowest level was the interface between Matlab and Marc Mentat (e.g. number of increments in the elevar subroutine). In Matlab, the lowest level where an error could occur was in the the opti_fmin file (in most cases an error was due to wrong definitions like the material matrix M (see Appendix B.2, line 25 and B.3, line 27 to 55)or the Marc Mentat simulation name). The F_eval file should not generate errors itself, as long as the dimensions

of the simu_result files are not changed and the M matrix set properly. Due to its large number of components M was the majors source of error. The final and top level where could occur an error, was the FCQ_file containing all mathematical formulations. These errors were address simply by plotting the results and checking the formulae. In general, it is recommended to start debugging either at the top or at the bottom level.

Note that optimisation algorithms implemented in Matlab always seek a minimum value not a maximum, but this minimum is represented by a maximum FCQ value in the following sections.

Before running a optimization it should always be checked:

(a) If in Marc Mentat the right subroutine was chosen (incl. the ”compile and save” - option).

(b) If COMMOM_VAR file path in the rebar subroutine is correct (Appendix C, line 50).

(c) If the increment number to write the output in the Elevar subroutine (Appendix C, line 228) is the same as the maximal number of increments set in Marc Mentat .

(d) If the right .dat file was generated by Marc Mentat.

3.4 Computational time and stability

Computational time is a key parameter when running an optimization. To obtain an accuracy lower than 1 °, between 50 and 120 optimization itera-

tions were necessary. So if one simulation iteration took two hours, the total run time of one optimization was more than two days. At Matlab level, calculation time was relatively negligible (Table 2).

In table 2 the average time of a total optimization iteration (Marc Mentat simulation and Matlab function evaluation) is presented for different cases.

Model	**Iterations**	**Total time**	**Matlab only**
Small model			
Semi-ring			
Compression	10	25.43s	0.38s
Traction	10	17.32s	0.38s
Complete model			
Extension	30	29min 60s	1.50s
Flextion	48	37min 24s	1.46s
Compression	48	31min 26s	1.51s
Torsion	48	22min 45s	1.48s

Table 2. Number of iterations and total time of one optimization iteration including simulation, writing and reading in the output files and evaluating the objective function. Due to strong non-linearities the small model was only run with 1000 iterations. Values were obtained by taking the average over several iterations. In any case values are only approximative because they depend on how many calculations are running in parallel.

Runtime had to by playing with the increment and solver parameters in Marc Mentat. This was done by decreasing the time step size to a minimum (until convergence was not achieved any more), benchmarking the solvers and implementing the most efficient one (Table 3). The following analyses types result in non-symmetric systems of equations: Inclusion of convective terms in heat transfer analysis, Coriolis effects in transient dynamic analysis, fluid mechanics, steady state rolling, soil analysis, follower force stiffness and

frictional contact. A symmetric solver was used, since it could approximate the problem solution and uses half as much memory for storing the stiffness matrix than non-symmetric solvers [43]and therefore less time.

Solver	Iterations [-]	Wall time [s]
Multifrontal sparse / non-sym.	150	∼4200
Multifrontal sparse / non-sym.	100	∼3200
Direct profile / non-sym.	150(14)*	∼6400
Mixed (iterative/direct) / sym.	150	1841
Direct sparse / sym.	150(N/A)*	17439
Casi iterative / sym.	150	4013
Hardware sparse / sym.	150	∼2500
Multifrontal / sym.	150	2580
Multifrontal / sym.	250	3829
Mixed (iterative/direct) / sym.	150	1841
Mixed (iterative/direct) / sym.	100	1825
Mixed (iterative/direct) / sym.	80	1628
Mixed (iterative/direct) / sym.	30(11)*	2800
Mixed (iterative/direct) / sym.	50	1300

Table 3. Solver benchmarking for a first version of complete model under extension ($\alpha_0 = 10\,^\circ$, $\nabla_r\alpha = 0\,^\circ$ and $\nabla_t\alpha = 50\,^\circ$).
** Simulation did not converge, in brackets the iteration number where the failure occurred.*

3.5 Verification, sensitivity and validation

First verification were about the newly implemented subroutine code, especially the rebar subroutine. Also the interface between Matlab and Marc Mentat, other new subroutine parts and m-files have to be validated. Moreover a mesh resolution convergence testing is necessary. For example, the cuboid mesh was set to be only a ”one” element (column) mesh. Therefore, in the context of this study, its limits in term of convergence are numerous

and discussed in Section 4.1.

Implemented optimization functions and parameter normalisation were initially tested using simple problems of known solutions.

Then, the sensitivity of the optimisation procedure to the parameters α_0, $\nabla_r \alpha$ and $\nabla_t \alpha$ was checked and discussed in result section 4.2.2.

Finally a comparison with AF fibre angle distributions was treated in the section 5.4.

3.5.1 Subroutine verification

As the code for to orientate the fibres was not trivial, a rigorous validation was necessary. The following controls were undertaken:

(a) Comparison between a model with and without subroutines: A fibre orientation was implemented manually in Mentat and then compared to an orientation generated by the rebar subroutine.

(b) Visual verification of the rebar output file: Global fibre orientations, local element errors, and fibre criss-cross pattern were checked using visual control (Fig. 8).

(c) Comparison of parameters at every iteration: Marc Mentat calls the rebar subroutine at every iteration, not just at the beginning of the simulation. Thus, at large deformations element coordinates had to be replaced by the coordinates plus the deformation to calculate the actual fibre orientation.

(d) Internal parameters of the subroutine code like material number, rotation matrices or relative element positions were verified writing the required data to text files.

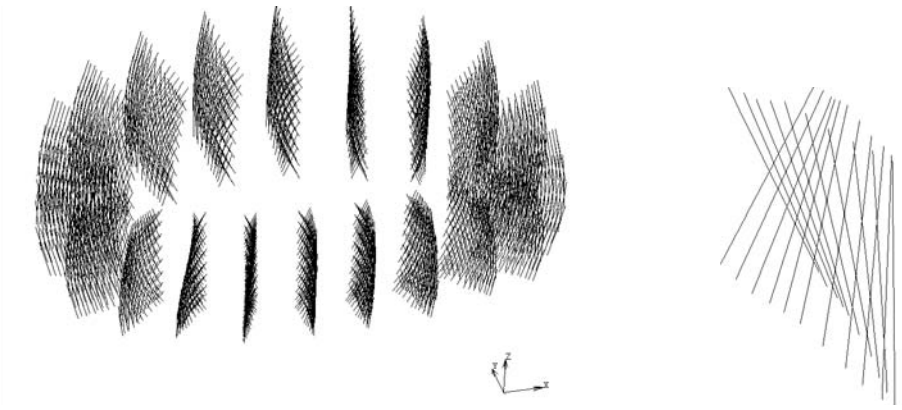

(a) (b)

Figure 8. The rebar output file permitted to verify visually fibre orientation a): AF b): zoom of a fibre layer in the anterior AF ($\alpha_0 = 0\,^\circ$ and $\sim \nabla_r \alpha = 30\,^\circ$)

Quantitative verification of the ordinary output files - the output of a simulation, which is read in by Matlab has to be the same, as the Marc Mentat ouput. Values were compared manually between the Marc Mentat output file and Matlab plots.

3.5.2 Matlab file verification

M-files were verified using single parameters of one element or layer (e.g. strain at an integration point), whose output was tracked through the files. It was assumed that if formulae or a process work with single values (e.g the first and the last), it will work with all the others, treating them in the

same way. Moreover, many procedures were validated by plotting results or writing them to the workspace.

3.5.3 Link between Matlab and Marc Mentat: Convergence issue

The basic functioning was controlled and verified manually by checking outgoing and incoming values.

More serious becomes the verification during the optimization process. Nonlinearity of the material properties, composite materials, large deformations and contact had a negative effect on FE simulation stability. Therefore the question how to control during an optimization whether on single FE simulation converged or not, became a main issue: Time step size and total number of time steps were constant and the output files ("simu_result_#" files) were always written at the same predefined time-step (see also 3.3.2). This allowed to have good control over convergence: When a simulation did not converge, evaluation function values do not change at all from one optimization iteration to the next [4] , because the simulation does not reach the final time-step. Therefore, at the end of an optimization it was always controlled whether two consecutive equal evaluation function values were obtained. Moreover a convergence control was achieved by checking the time needed for one simulation. It is possible that one simulation duration may be higher than the average duration (e.g. tab.2), but in case of large differences convergence was controlled by running a simulation at the point (α_0, $\nabla_r \alpha$ and $\nabla_t \alpha$), where the instability had been suspected.

[4] At an evaluation function error of 10^{-5} the probability that the values form two consecutive optimization iterations are the same is $1{:}10^{10}$.

4 Results and discussion

The result section is structured into three main part according to the three used FE geometries. Moreover, results have do be differentiated by function evaluations ($\overline{FCQ}$ values at given fibre orientations consisting in α_0, $\nabla_r\alpha$ and $\nabla_t\alpha$) and complete optimisations consisting in an initial and a final fibre orientation and an optimisation path.

4.1 Cuboid model

Problems occurred in terms of convergence. However, the model was useful to introduce different result representations and discuss convergence.

4.1.1 Result representation

To prove that a global minima or maxima of the $\overline{FCQ}$ function was really global, all possible solutions had to be tested. A four-dimensional representation would be necessary to present a value (e.g. $\overline{FCQ}$) at each point of the three-dimensional solution space (α_0, $\nabla_r\alpha$ and $\nabla_t\alpha$). This was too complicated and would have required a huge amount of function evaluations. Therefore, three simplified options were chosen:

(a) Surfaces or contour plots taking into account two optimization directions (e.g. Fig. 9 and 10).

(b) XY-plots in the three directions varying on parameter and keeping the other two constant (e.g. $\alpha_0 = [0\,°;90\,°]$ $\nabla_r\alpha = \nabla_t\alpha = 0$, Fig. 11)

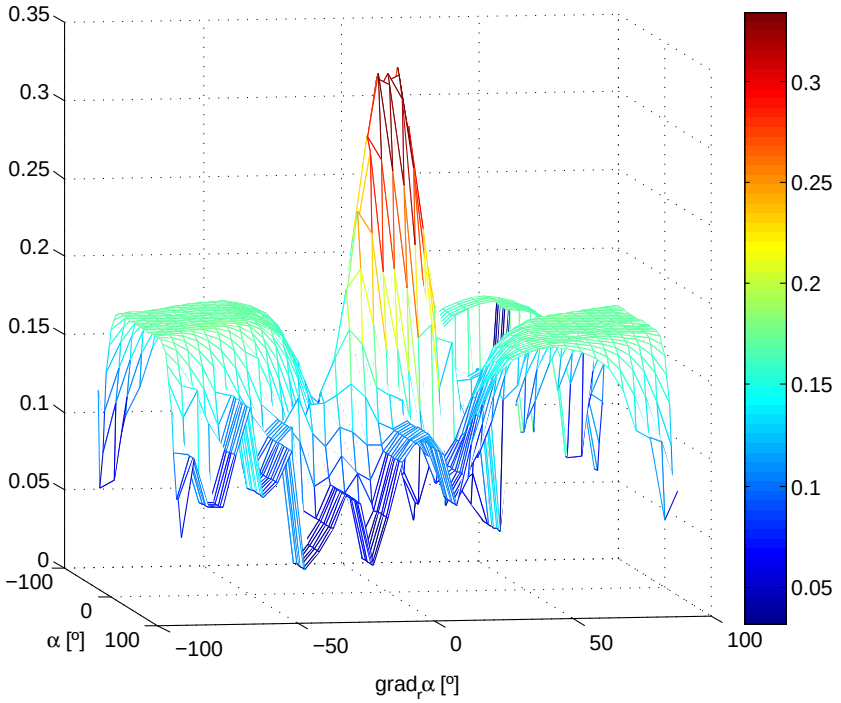

Figure 9. Surface representation of $\overline{FCQ}$ (z axis & colour bar) values in function of α_0 and $\nabla_r\alpha$. Cuboid model under uni-axial traction (total strain of 10%).

(c) Optimization path plots in two directions (Example in Section 4.3)

As the computational time was higher to produce a surface or a contour. In case of the L4-L5 segment geometry results will be presented only using option (b) or (c) and as in this report only optimisations run on the L4-L5 segment geometry were presented, option (c) will only be used in Section 4.3.

Option (b) was not very self explaining. In fact it consisted of one, two or three slices of a surface or contour intersection in a region of interest. Each plotted line represents one direction of the solution space changing one parameter and keeping the others constant. A step by step example was

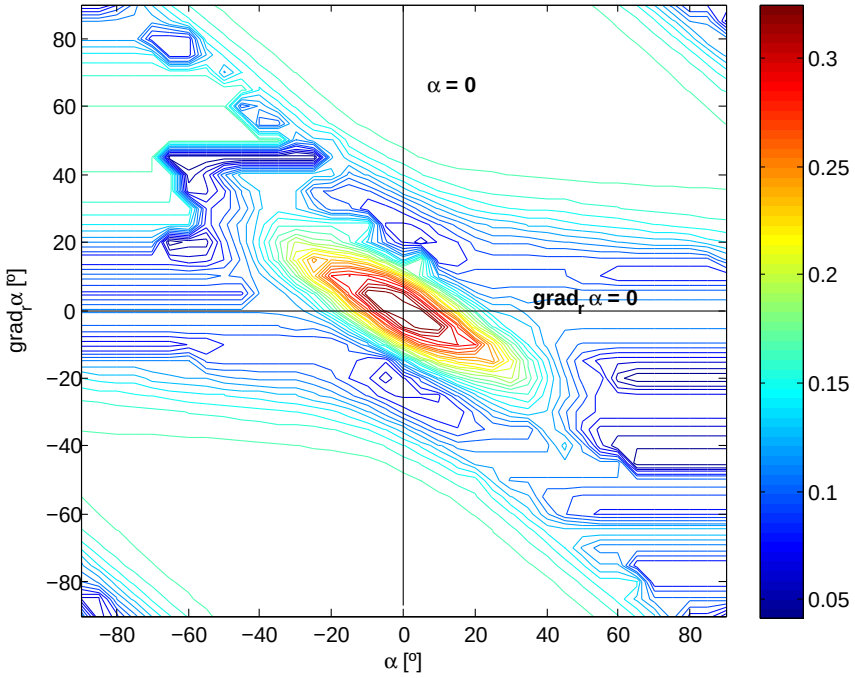

Figure 10. The surface of Figure 9 represented as contour plot. $\overline{FCQ}$ (colour bar) values in function of α_0 and $\nabla_r\alpha$. Cuboid model under uni-axial traction (total strain of 10%. The black lines indicate the same data as presented in figure 11.

created in Figure 11: Under traction, the region of interest is $\alpha_0 = 0\,^\circ$ and $\nabla_r\alpha = 0\,^\circ$, since the maximal $\overline{FCQ}$ value was expected to be at this point. The two intersecting lines in the contour plot (Fig. 10) were redrawn varying α_0 while keeping $\nabla_r\alpha$ constant (Fig. 11a) or varying $\nabla_r\alpha$ while keeping α_0 constant (Fig. 11a). Both were placed into one graph (Fig. 11c) and then, as the solution was symmetric, just only half of the plotted lines was reproduced (Fig. 11d). Note that in the cuboid geometry no $\nabla_t\alpha$ existed. In later plots $\nabla_t\alpha$ will be drawn as an own direction.

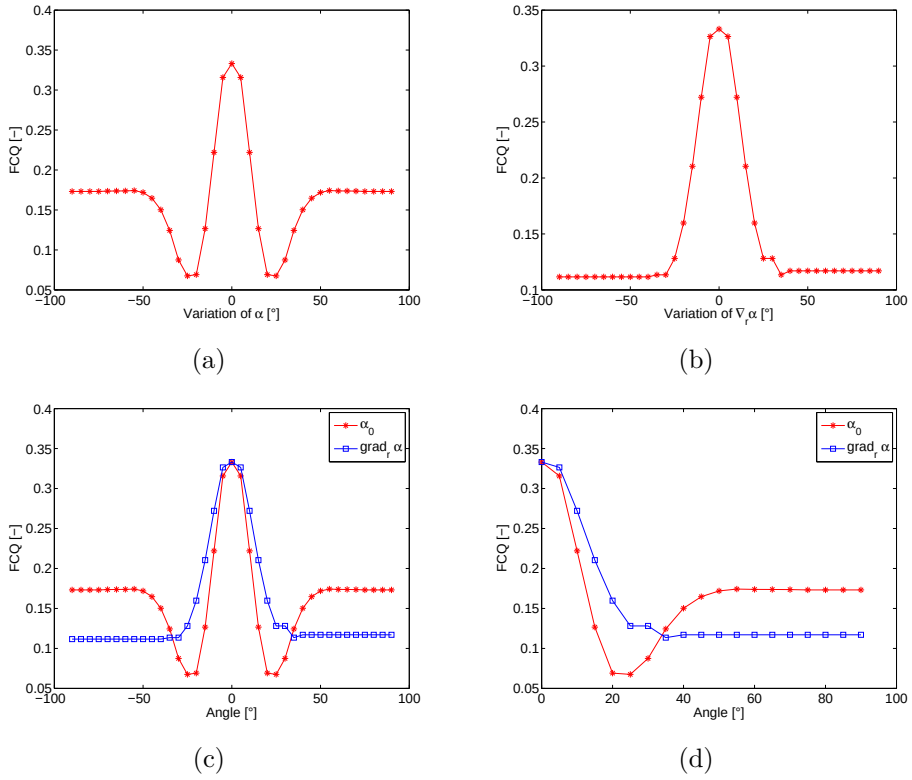

Figure 11. $\overline{FCQ}$ values of the small model under uni-axial traction (total strain of 10%). Each point represents one FE simulation a): varying α_0 while keeping $\nabla_r\alpha = 0$ and b) varying $\nabla_r\alpha$ while keeping $\alpha_0 = 0$ c): both put together in the same graph d): only the positive part of the solution.

In some cases, especially for the L4-L5 model, graphs are no more symmetric around a minima or maxima and both positive and negative directions will be reproduced (Example in Section 4.3.1 in Figure 19d).

4.1.2 FCQ values and convergence

Figure 10 had a lot of irregularities, abrupt $\overline{FCQ}$ changes and local $\overline{FCQ}$ minima. It will be demonstrated in the next section that some of these

irregularities were due to boundary conditions. However, more important were all the flat contour lines (parallel to the $\nabla_r \alpha$ axis). A flat line meant having a constant value in one direction. This was simply not possible to such an extend and indicated non-converged simulations (Section 3.5.3).
Although simulations with 1000 increments were run at each point about 50 and 75% of the simulations did not converge. As a change of fibre angle within a single element from almost 0 to 90 degree is huge was simulated, convergence problems are not surprising, but showed that the stability of the used unconstrained optimisation procedure depended on mesh refinement.'0

4.2 Semi cylinder

First, the obtained results of the $\overline{FCQ}$ objective function and its parameters will be presented and in a second stage using a benchmarking it was explained why the current $\overline{FCQ}$ function had been chosen.

4.2.1 RMS, MSE, RSD and FCQ results

In Figure 12 $\overline{RMS}$ values in the semi-ring are presented. Under compression, the maximal fibre stresses were computed at $\alpha_0 = 90\,^\circ$ with $\nabla_r \alpha = 0\,^\circ$ and $\nabla_t \alpha = 0\,^\circ$ and under traction at $\alpha_0 = 0\,^\circ$ with $\nabla_r \alpha = 0\,^\circ$ and $\nabla_t \alpha = 0\,^\circ$ which were the expected maxima.
Under compression, for a constant fibre orientation with α_0 between $0\,^\circ$ and $32.5\,^\circ$) the $\overline{RMS}$ value was practically zero. This indicated that in the given interval the fibres are practically unused. Bellow a constant fibre orientation of $\sim 62\,^\circ$ fibre stresses are bellow 0.1. Under traction, at an absolute fibre

angle over ∼62 ° $\overline{RMS}$ values are below 0.1 and become completely negligible over 80 °.

$\overline{MSE}$ or matrix shear strain parameter values are presented in Figure 13.

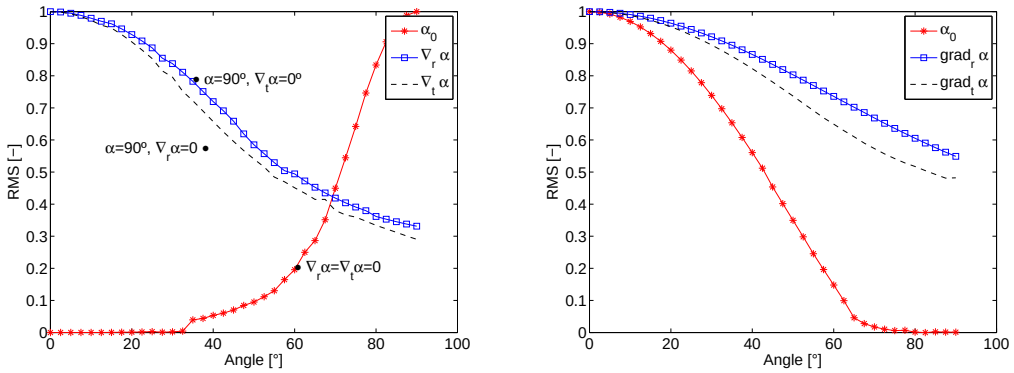

(a) Compression (b) Traction

Figure 12. Radial Mean Stress ($\overline{RMS}$) respectively averaged fibre stress values. One direction (α_0,$\nabla_r\alpha$ or $\nabla_t\alpha$) was varied while keeping the other two constant. a): axial compression - zone of interest: $\alpha_0 = 90\,°$, $\nabla_r\alpha = 0\,°$ and $\nabla_t\alpha = 0\,°$ b): axial traction - zone of interest: $\alpha_0 = 0\,°$, $\nabla_r\alpha = 0\,°$ and $\nabla_t\alpha = 0\,°$.

Under compression, minimum values were obtained at a fibre orientation of $\alpha_0 = 90\,°$ with $\nabla_r\alpha = \nabla_t\alpha = 0\,°$. At a constant angle of $\sim \alpha_0 = 32.5\,°$ matrix strain values suddenly rose. This also happened in the case of $\overline{RMS}$, but its sudden decrease was less visible. This was further further illustrated in Section 4.2.3.

Under traction, maximal fibre stress did not imply minimal matrix shear strain: minimal $\overline{MSE}$ values were either around α_0 =∼27 ° or over α_0 =∼70 °.

To understand the behaviour of the $\overline{RSD}$ parameter, i.e. the radial stress distribution parameter, first the effective radial stress have to be presented. In Figure 14 and 15, fibre stresses through the tissue thickness in the anterior

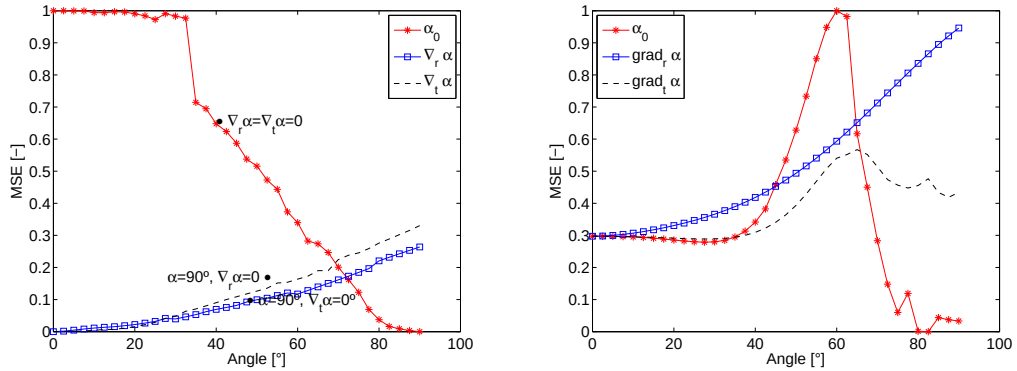

(a) Compression (b) Traction

Figure 13. Matrix Shear Stress ($\overline{MSE}$). One direction (α_0,$\nabla_r\alpha$ or $\nabla_t\alpha$) was varied while keeping the other two constant. a): axial compression - zone of interest: $\alpha_0 = 90\,^\circ$, $\nabla_r\alpha = 0\,^\circ$ and $\nabla_t\alpha = 0\,^\circ$ b): axial traction - zone of interest: $\alpha_0 = 0\,^\circ$, $\nabla_r\alpha = 0\,^\circ$ and $\nabla_t\alpha = 0\,^\circ$.

section were presented (all sections - anterior, lateral, etc. - have the same shape in case of compression or traction). To compute the $\overline{RSD}$ values, a second order polynomial was fitted to the stress values (Eq. 5).

Figure 16 showed $\overline{RSD}$ values. $\overline{RSD}$ was maximal for optimal fibre orientations. As the aim was to minimize the parameter $\overline{RSD}$ this was not really expected. Yet, when comparing $\overline{RSD}$ values to the radial strain distributions (fig.14 and 15) this would be explained: As coefficient "a" weight four times that of "b" (Eq. 4) under traction (compression) $\overline{RSD}$ values will be highest at $\alpha_0 = \nabla_r\alpha = \nabla_t\alpha = 0\,^\circ$ ($\alpha_0 = 90\,^\circ$ and $\nabla_r\alpha = \nabla_t\alpha = 0\,^\circ$) because also "a" reached its maximal value at the same point. In function of $\nabla_r\alpha$ under traction and compression $\overline{RSD}$ was maximal at $\nabla_r\alpha = 0$, reached a minimum around $45\,^\circ$ and increased again toward $90\,^\circ$. As fibre distribution around $\nabla_r\alpha = 45\,^\circ$ was nearly linear (Fig. 14b and 15b) this could be explained.

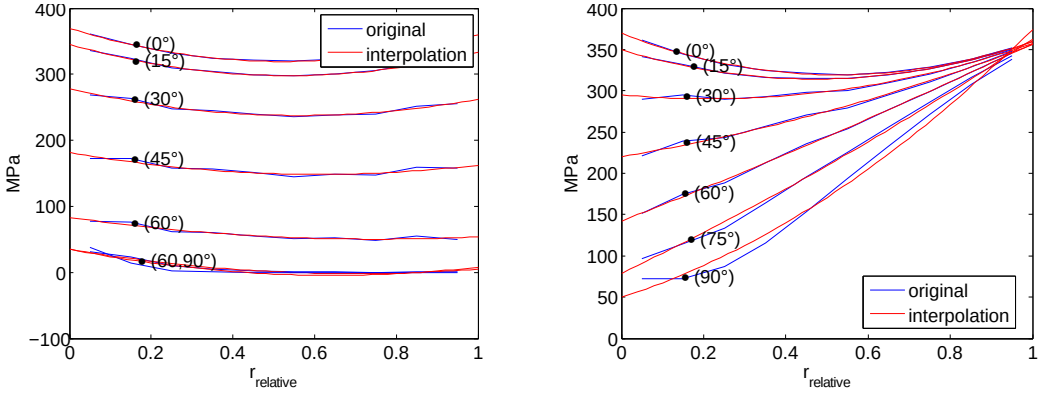

(a) Varying α (b) Varying $\nabla_r \alpha$

Figure 14. Fibre stress* distribution through the tissue thickness under traction and the fitted parabolic curves. $r_{relative} = 0$ is the outermost fibre and $r_{relative} = 1$ in the innermost fibre.
*One fibre is defined by a layer of four integration point $\Rightarrow$ to obtain the absolute fibre stresses values have to be divided by four.

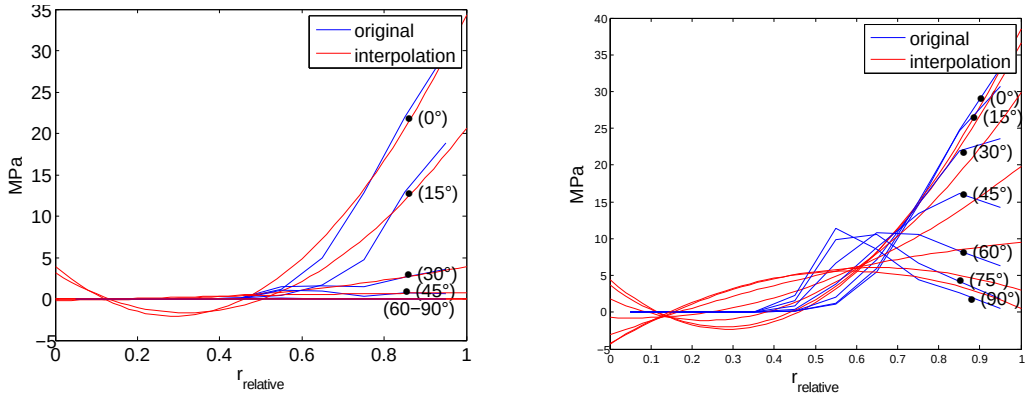

(a) Varying α (b) Varying $\nabla_r \alpha$

Figure 15. Fibre stress* distribution through the tissue thickness under compression and the fitted parabolic curves. $r_{relative} = 0$ is the outermost and $r_{relative} = 1$ the innermost fibre.
*One fibre is defined by a layer of four integration point $\Rightarrow$ to obtain the absolute fibre stresses values have to be divided by four.

Relevance of this results out of a biological perspective were treated in the discussion.

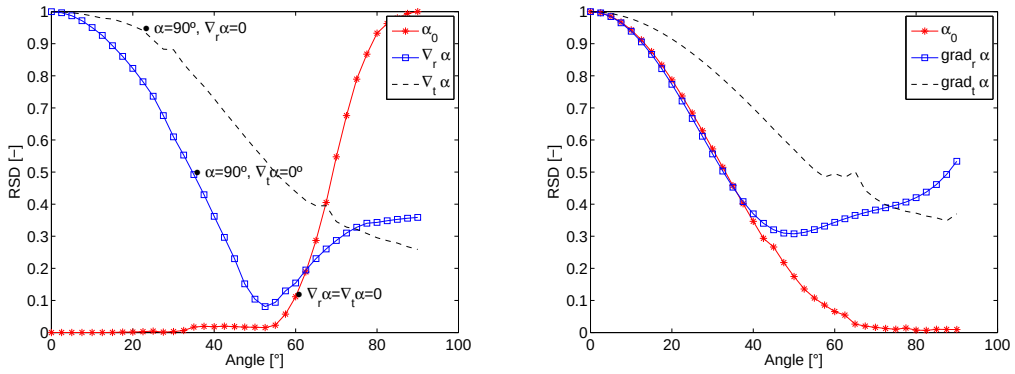

(a) Compression (b) Traction

Figure 16. Radial Stress Distribution ($\overline{RSD}$). One direction (α_0,$\nabla_r\alpha$ or $\nabla_t\alpha$) was varied while keeping the other two constant. a): axial compression - zone of interest: $\alpha_0 = 90\,^\circ$, $\nabla_r\alpha = 0\,^\circ$ and $\nabla_t\alpha = 0\,^\circ$ b): axial traction - zone of interest: $\alpha_0 = 0\,^\circ$, $\nabla_r\alpha = 0\,^\circ$ and $\nabla_t\alpha = 0\,^\circ$.

Finally the $\overline{FCQ}$ parameter was plotted in Figure 17. It predicted better fibre orientations around a constant fibre angle of 45 ° for compression and traction. As for traction and compression a internal pressure was applied, function evaluations were repeated without internal pressure. Although values changed slightly the same minima and maxima of $\overline{FCQ}$, $\overline{RMS}$, $\overline{MSE}$ and $\overline{RSD}$ were found.

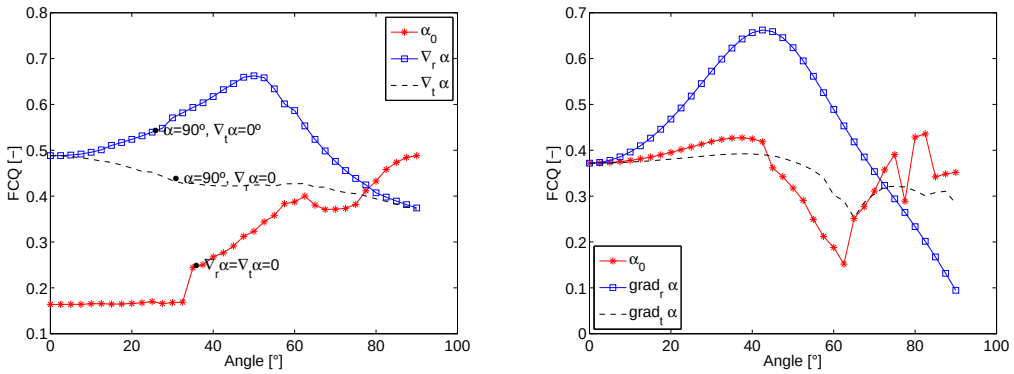

(a) Compression (b) Traction

Figure 17. Fiber contribution Quality ($\overline{FCQ}$). One direction(α_0,$\nabla_r\alpha$ or $\nabla_t\alpha$) was varied while keeping the other two constant. a): axial compression - zone of interest: $\alpha_0 = 90\,°$, $\nabla_r\alpha = 0\,°$ and $\nabla_t\alpha = 0\,°$ b): axial traction - zone of interest: $\alpha_0 = 0\,°$, $\nabla_r\alpha = 0\,°$ and $\nabla_t\alpha = 0\,°$.

Concerning $\nabla_t\alpha$, $\overline{FCQ}$ and its parameters according to the symmetry of both loads and geometry. In both load cases and for all $\overline{FCQ}$ parameters slops of the plotted lines were steeper for α_0 than for $\nabla_r\alpha$ and $\nabla_t\alpha$ meaning that optimisation convergence along α_0 would be faster than along $\nabla_r\alpha$ and $\nabla_t\alpha$.

4.2.2 Parameter benchmarking

A benchmarking was done for $\overline{MSE}$ and $\overline{RSD}$. Three versions of $\overline{MSE}$ were tested using either sum of total shear strains ($\sum |\varepsilon_{ij}|, i \neq j$), the sum of maximal shear strains ($\sum |\frac{\varepsilon_I - \varepsilon_{III}}{2}|$) or the sum of shear stresses in only z direction ($\sum |\varepsilon_{13}|$). No significant differences were found since the aim of the $\overline{MSE}$ parameter was to track loads of the extracellular matrix the maximal shear strain was kept. The benchmarking results are presented in Appendix A.0.3.

Among all three parameters contribution to the $\overline{FCQ}$ values, $\overline{RSD}$ was the most complex parameter. Initially, it had the form $\sum_t \sqrt{4a_t^2 + b_t^2} / \sum \sigma_t$ which results in a division by zero in case of no fibre stress in all fibres of a segment. Therefore, it was changed to $\sum_t \sqrt{4a_t^2 + b_t^2} / (\sum \sigma_t + 1)$ to avoid these problem. In a final step it was changed to $\sum_t \sqrt{4a_t^2 + b_t^2}$ arguing that stress gradient values should be absolute values and not relative to the sum of total fibre stress in tangential section. Introducing this last change a over evaluation of weakly loaded fibres could be avoided. The second and the third version were presented in Figure 18. Moreover, further $\overline{RSD}$ formulations were presented, but as there was no time to thoroughly explore them, they will only be part of the general discussion.

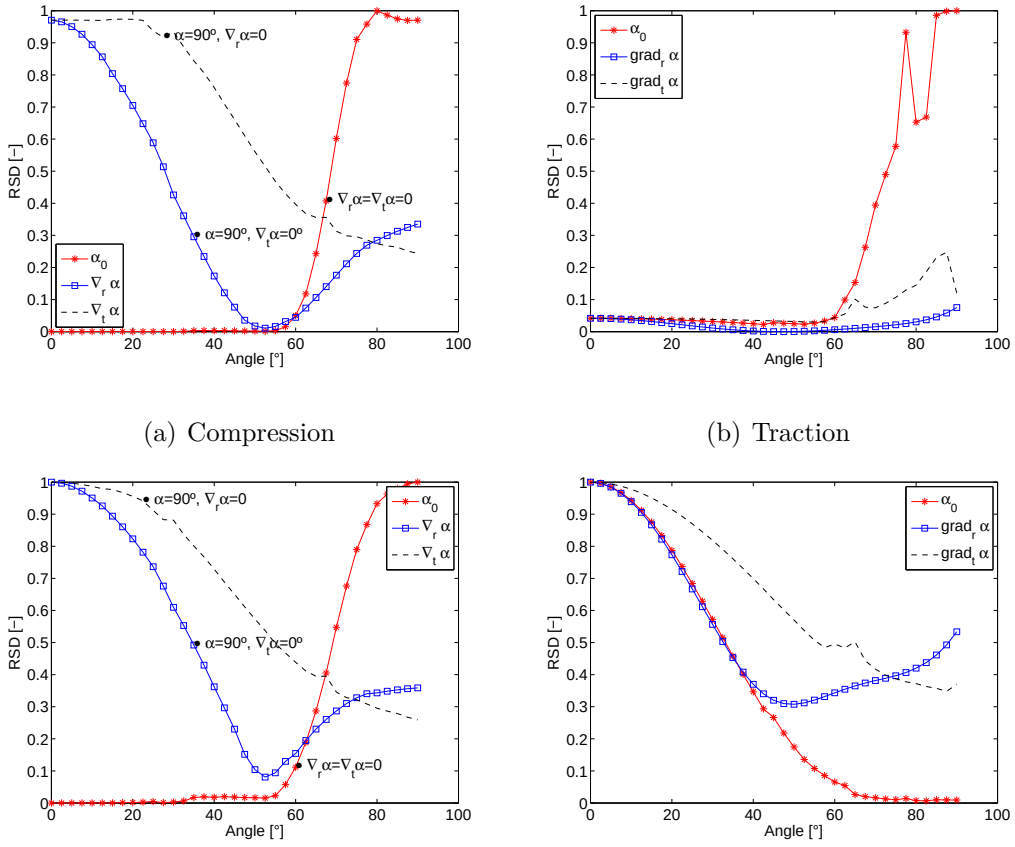

(a) Compression (b) Traction

(c) Compression (d) Traction

Figure 18. RSD benchmarking. One direction(α_0,$\nabla_r\alpha$ or $\nabla_t\alpha$) was varied while keeping the other two constant. a) and b): $RSD = \frac{\sqrt{4a_t^2+b_t^2}}{\sum_t \sigma_t+1}$ c) and d): Final RSD $\sum_t \sqrt{4a_t^2+b_t^2}$.

4.2.3 Critical angle

At a given angle, the fibre strain became negative and so the fibre stress was equal to zero. When this happened abruptly in many different fibres a sudden increase or decrease ((Fig. 13)a). This sudden change was found to be situated between a fibre angle of 33 ° and 33.4 ° (under traction between

56.6° and 57°). However, this explains these shifts which occurred for in case of all $\overline{FCQ}$ parameters.

Several different types of optimisations were run on the semi-cylinder geometry mainly to test an verify the program structure. As these optimisations only gave one result in function of one initial point, but did not contribute to a better understanding of the overall $\overline{FCQ}$ function and its parameters, non of the optimisation results is presented here.

4.3 Complete L4-L5 segment model

The optimisation results presented bellow were all obtained in the case of a runtime of iterative $\overline{FCQ}$ function evaluations which correspond to approximately one day of calculations. The initial position (e.g. $\alpha_0 = 40°$, $\nabla_r\alpha = 10°$ and $\nabla_r\alpha = -20°$) was chosen by evaluating about 25 points along the axis α_0, $\nabla_r\alpha$ and $\nabla_r\alpha$, which also served to set the initial maximal and minimal parameter values of the $\overline{FCQ}$ parameters. In the figures in this section the results are either presented in terms of optimisation path (sub-figures a and b), change of the $\overline{FCQ}$ parameters during the optimization (sub-figure c) or in terms of deviation from the final encountered $\overline{FCQ}$ maximum (sub-figure d). Last was computed after the optimization was finished: In direction α_0, $\nabla_r\alpha$ and $\nabla_t\alpha$ several points around the maximum were evaluated and plotted, which permitted to verify whether a maximum value was global or local.

4.3.1 Flexion

With an initial position of a constant fibre angle of 35 °$\overline{FCQ}$ was found to be maximal at $\alpha_0 = 32.2\,^\circ$ and $\nabla_r\alpha = \nabla_t\alpha = 0\,^\circ$. Neither radial or tangential gradients were found thought a positive gradient was expected in tangential direction, due to the compression in the anterior annulus and the traction in the posterior. High fibre stresses ($\overline{RMS}$) were obtained together wit high matrix shear stresses $\overline{MSE}$. A complete example of stress distribution in all segments of the AF is given in Appendix A.0.4

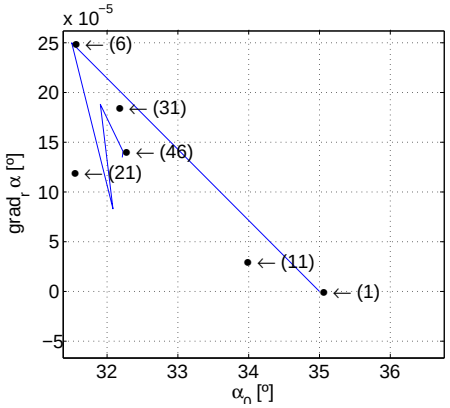

(a) Evolution of $\alpha_0/\nabla_r\alpha$

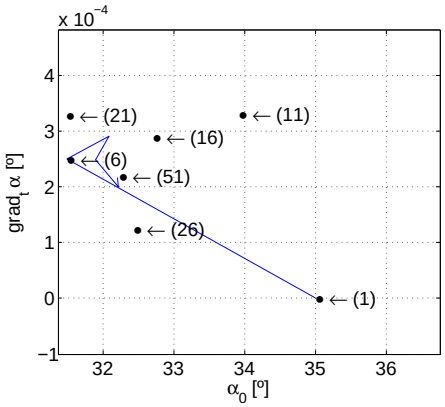

(b) Evolution of $\alpha_0/\nabla_t\alpha$

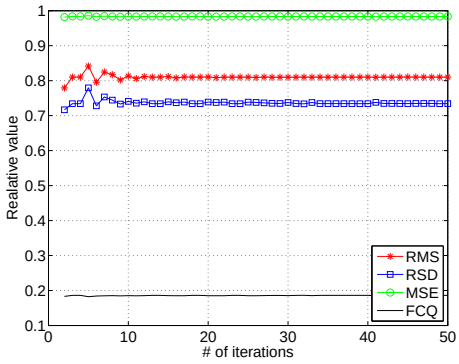

(c) Parameter evolution

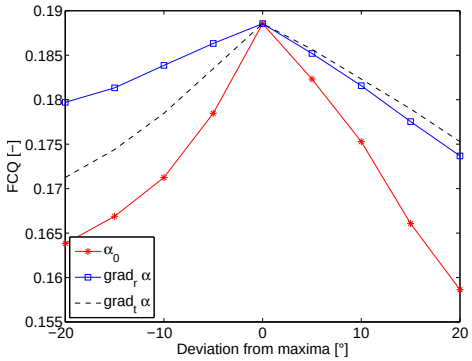

(d) Maxima validation

Figure 19. Tracking of an optimization - L4-L5 under flexion (6 Nm). a) and b) evolution of the optimization in the three different directions. Black points indicate some function evaluations (one simulation) and the blue line the final path. c) evolution of $\overline{RMS}$, $\overline{RSD}$, $\overline{MSE}$ and $\overline{FCQ}$ d) the maxima was checked in all three direction over a radius of $\pm$ 20 °.

4.3.2 Extension

$\overline{FCQ}$ converged to $\alpha_0 = 52.5\,^\circ$ and $\nabla_r\alpha = \nabla_t\alpha = 0\,^\circ$. As for flexion no tangential nor radial gradient was found. A negative gradient was expected.

In this initial (constant $\alpha = 52\,°$) value was not as good as expected and the algorithm hat to find the maximum over a path of 15 degree. A solution with low matrix shear strain (low $\overline{MSE}$) was favoured in respect to a high $\overline{RMS}$ value.

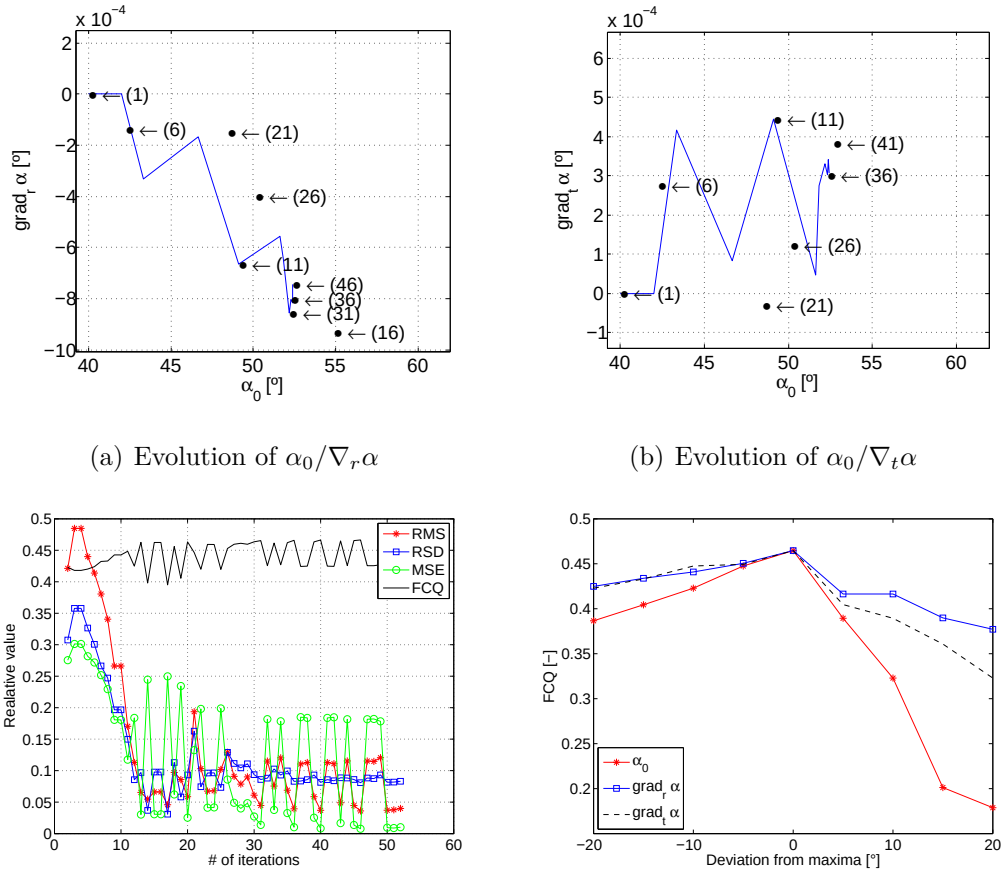

(a) Evolution of $\alpha_0/\nabla_r\alpha$

(b) Evolution of $\alpha_0/\nabla_t\alpha$

(c) Parameter evolution

(d) Maxima validation

Figure 20. Tracking of an optimization - L4-L5 under extension (10 Nm). a) and b) evolution of the optimization in the three different directions. Black points indicate some function evaluations (one simulation) and the blue line the final path. c) evolution of $\overline{RMS}$, $\overline{RSD}$, $\overline{MSE}$ and $\overline{FCQ}$ d) the maxima was checked in all three direction over a radius of $\pm$ 20 °.

4.3.3 Torsion

Under torsion (9 Nm), the optimal fibre orientation found was $\alpha_0 = -2.0\,^\circ$, $\nabla_r\alpha = 32.0\,^\circ$ and $\nabla_t\alpha = 0.0\,^\circ$. There was no time to validate the solution and the optimisation only brought few information, since the algorithm declared the initial position as the solution. However values seem to be correct, according to the presence of coupled axial disc stretching.

4.3.4 Compression

Under compression, the algorithm converged to $\alpha_0 = 64.6\,^\circ$, $\nabla_r\alpha = 10.3\,^\circ$ and $\nabla_t\alpha = 0\,^\circ$. During the optimisation, $\overline{RMS}$ was forced to decrease. However, a decreased $\overline{MSE}$ value was obtained. There was no time to validate the minimum. Before a minimum around $\alpha_0 = 80\,^\circ$, $\nabla_r\alpha = 0\,^\circ$ and $\nabla_t\alpha = 0\,^\circ$ was found and during the verification discovered to be local.

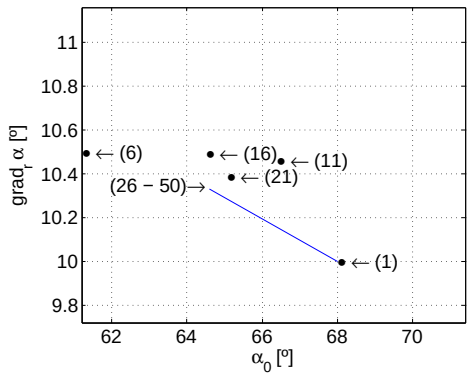

(a) Evolution of $\alpha_0/\nabla_r\alpha$

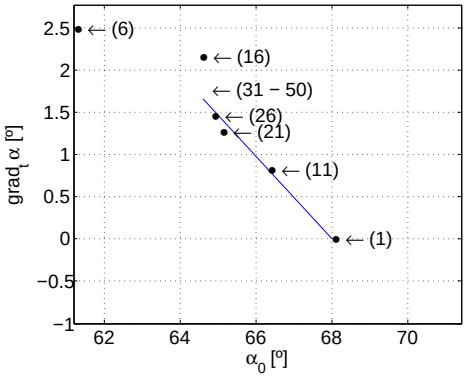

(b) Evolution of $\alpha_0/\nabla_t\alpha$

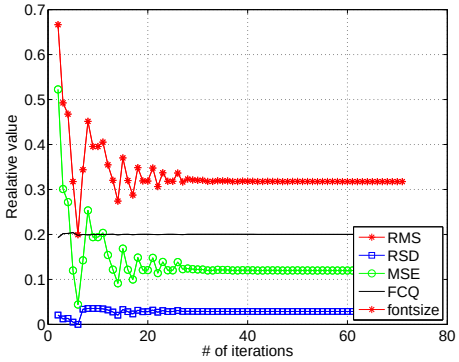

(c) Parameter evolution

Figure 21. Tracking of an optimization - L4-L5 under compression (0.38 MPa). a) and b) evolution of the optimization in the three different directions. Black points indicate some function evaluations (one simulation) and the blue line the final path. c) evolution of $\overline{RMS}$, $\overline{RSD}$, $\overline{MSE}$ and $\overline{FCQ}$.

5 General discussion

5.1 Geometry and simulations

With respect to the cuboid geometry, results clearly showed that several elements are necessary (in radial and tangential direction) to explore fibre orientations changes. Therefore, the cuboid could only serve for program construction and verification purposes.

Concerning the semi-cylinder model, the probably most important issue is up to which extend the geometries used for the $\overline{FCQ}$ evaluation were the right choice. Under traction practically all obtained results were physically coherent (e.g. the stress distribution fig. 14). As long as α_0 was constant stress distribution through tissue thickness was also constant. When a gradient was introduced also the distribution becomes non-uniform.

More complicated to interpret are the results under compression (Fig. 15). Due to the internal pressure at any fibre angle or distribution, the inner fibres were more stressed than the outer. Yet, the outer fibres were completely unstressed in practically any position. This indicates that strains in the t direction (the plane the fibres are orientated) were still insufficient to generate stresses in the non-linear elastic fibres. This will be taken up again and further explained in section 5.6.

In the complete L4-L5 lumbar spine segment model a bizarre result with respect to fibre stress distribution occurred at three pairs of consecutive integration points, where stress values remained constant (Fig. 22). Such a stress distribution was thought to be caused by the irregular criss-cross pattern. Yet, as this pattern was always respected the result could not be ex-

plained. It could be due to the internal fibre stress calculation implemented in Marc Mentat.

5.2 Fibre Contribution Quality

In Table 4 the implemented $\overline{FCQ}$ changes over time of the different parameters are presented.

#	Improvement	Justification
1	RMS, MSE and RSD parameter scaling between 0 and 1	All parameters have the same weight in the $\overline{FCQ}$ formulation (Eq. 8)
2	$RSD = \sum_t \frac{\sqrt{4a_t^2 + b_t^2}}{\sum \sigma_t} \Rightarrow \sum_t \frac{\sqrt{4a_t^2 + b_t^2}}{\sum \sigma_t + 1}$	Avoid division by zero
3	$MSE = \sum \lvert\varepsilon_{ij}\rvert, i \neq j \Rightarrow \sum \lvert\frac{\varepsilon_I - \varepsilon_{III}}{2}\rvert$	Respects objectivity
4	$RSD = \sum_t \frac{\sqrt{4a_t^2 + b_t^2}}{\sum \sigma_t + 1} \Rightarrow \sum_t \sqrt{4a_t^2 + b_t^2}$	Attribute a higher importance to absolute than to relative values
5	$F(\sigma_{i,element}, \overline{r})$ (Eq. 5) $\Rightarrow F(\sigma_{i,fibre}, \overline{r})$	increase accuracy

Table 4. Historical overview of introduced enhancements

In the beginning, the parameters had to be averaged to have the same weight within the $\overline{FCQ}$ formulation. This was simply done introducing the maximum and minimum values (Eq. 7) for a given geometrical model. It was tried to set maxima and minima as close as possible to the their real global maxima or minima parameters (for one load case). However, if using minima and maxima of only a predefined zone of interest (e.g. only biologically admissible orientations $10\,° < \alpha < 70\,°$) results would be different. An

other possibility would also be to use minima and maxima values of all load cases. Yet, for example in case of a torsion a $RMS_{min} = 0$ (no stress in any fibre) can never occur. Therefore, the the last option was not considered to be valid.

RMS and MSE values were quite simple to model and explore. However the RSD parameter was more difficult to treat and to model correctly. Several problems occurred and had to be addressed during the FCQ parameter benchmarking part (4.2.2). An other important enhancement was the use of each fibre stress value and not fibre stress averaged over an element (in the table above improvement # 5). Instead of fitting a curve to a number of values equal to the number of elements in the r direction, one value per fibre layer was used which permitted to get a much better idea about the real radial fibre stress distribution in the AF and obtain better quality of parameter "a" and "b" (Eq. 3).

Despite the improvements the final results for $\overline{RSD}$ are still not very satisfying. When comparing values form Figure 14 and 16 the results could be correctly correlated on a mathematical base. Yet, for example when comparing stress distributions in the case of a changing gradient (Fig. 14 b) and their $\overline{RSD}$ values (Fig. 16 b), intuitively or out of the cell's perspective the distribution with a 60 degree radial gradient is "worse" than the one with 0 degree, but the 60 degree gradient led to better $\overline{RSD}$ evaluation. This over or under evaluation of certain orientations is due to the four times higher weight of parameter "a" in respect to "b" (Eq. 4).

However, as the RSD parameter was designed to equilibrate local fibre stress distribution in the real AF, it is probable that those mainly complex distri-

butions could not be simulated by the simple semi-cylinder model. Therefore further evaluation is necessary.

An other formulation for RSD could be the variance or r of each tangential section $var(r)_t$ (Fig. 24). This would take into account all local deviations, but still give penalties to "bad" global evaluations.

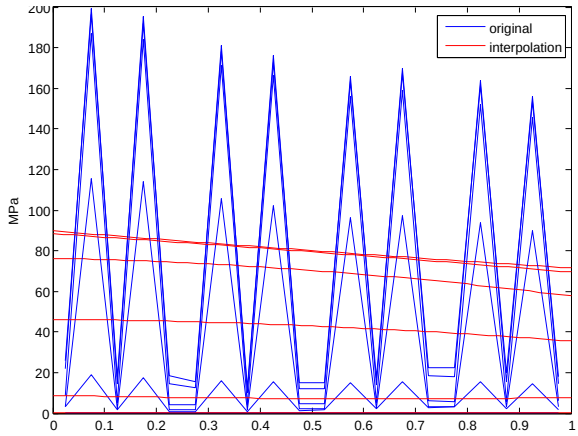

Figure 22. Latera AF segment under torsion: Fibre stress distribution from the outer to the inner AF.

A second option would be to simply leave away the RSD parameter. This could be justified by the fact that a "bad" distribution will induce higher matrix shear strains and therefore MSE values. Thus, the RSD parameter could somehow be included into MSE, but should first be verified using the real lumbar spine model.

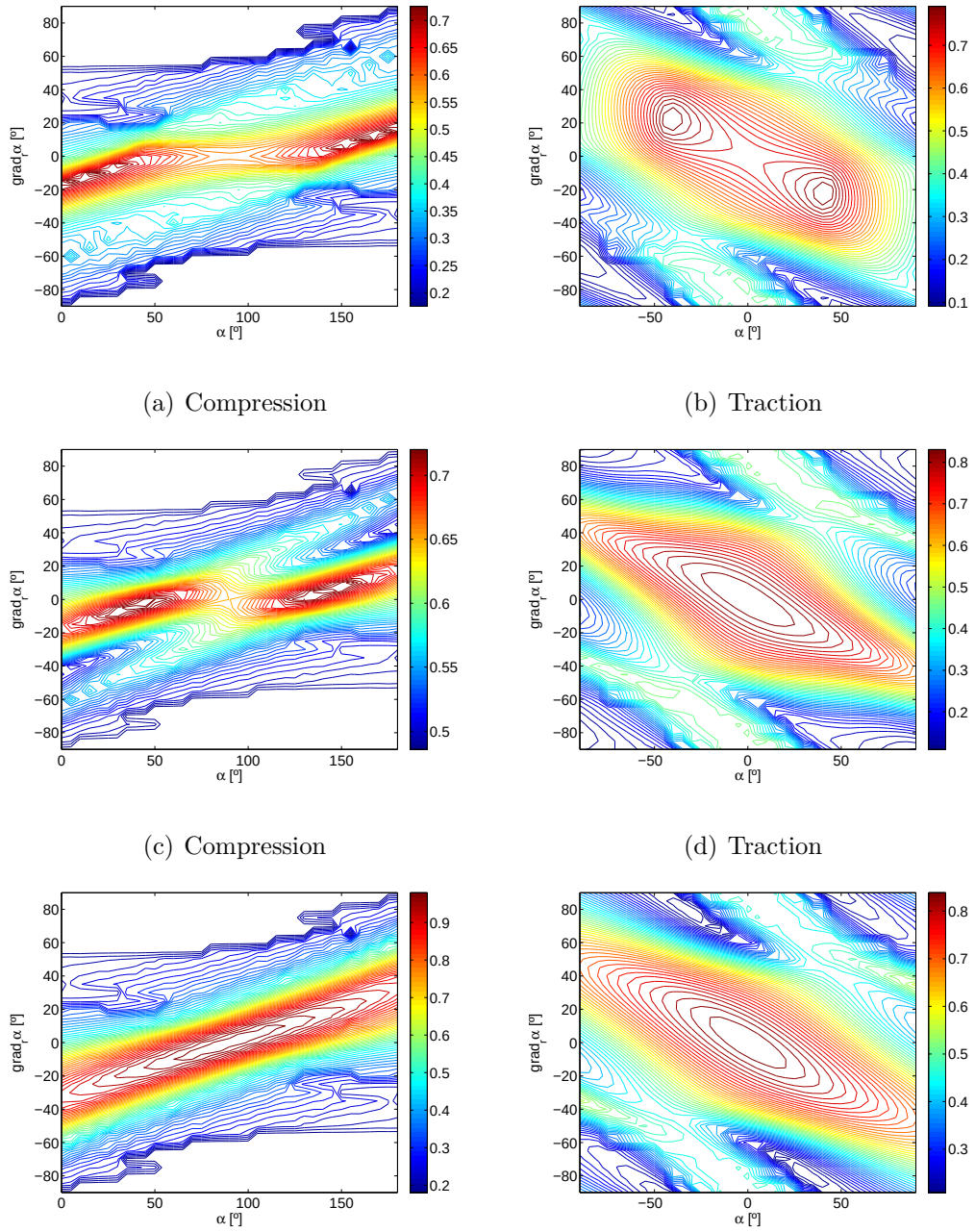

(a) Compression

(b) Traction

(c) Compression

(d) Traction

(e) Compression

(f) Traction

Figure 23. $\overline{FCQ}$ values in function of α_0 and $\nabla_r\alpha$ a) and b): Modified $\overline{FCQ}$ used for all simulations ($RSD = \sum_t \sqrt{4a_t^2 + b_t^2}$) c) and d): Introducing the variance. $RSD = \sum_t var(\sigma_t)$. where σ_t is the variance over a tangential segment e) and f): $\overline{FCQ}$ without $\overline{RSD}$ only in function of $\overline{RMS}$ and $\overline{MSE}$.

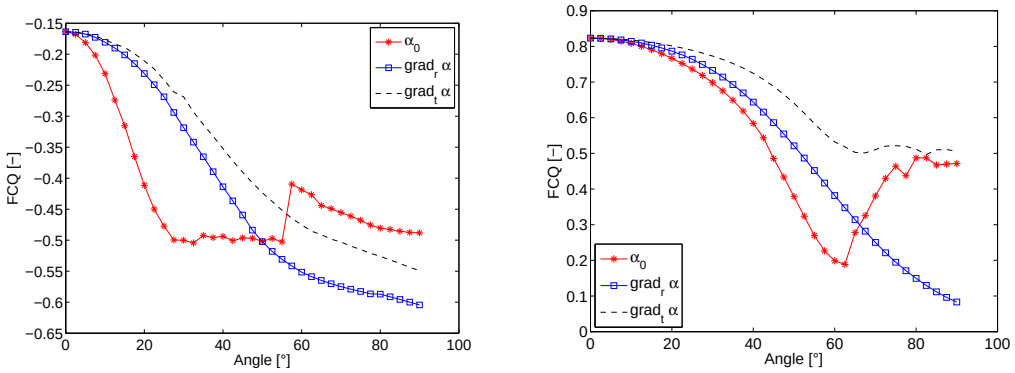

(a) Compression (b) Traction

Figure 24. FCQ using the variance of each tangential segment as RSD value.

Nevertheless, both proposed enhancements were first evaluated on the semi-cylinder (Fig. 23). The $\overline{FCQ}$ without $\overline{RSD}$ was the only formulation to explain properly the expected $\overline{FCQ}$ maximum under compression and traction (Fig. 23e,f). The variance FCQ-version showed good performance (Fig. 24), but could only explain the maximum under traction (Fig. 23c,d). Therefore, taking into account the somehow strange distribution under compression, the variance-based FCQ could be a good candidate to be explored.

5.3 Methods

In order to optimize the FE simulation convergence and computational cost, direct integration was chosen. There, one issue arose: Direct integration techniques are imprecise; this is true regardless of the discretisation technique is used. Each technique exhibits at least one of the following problems: conditional stability, artificial damping, and phase errors. Two computa-

tional drawbacks of the Houbolt operator are the requirement of a special starting procedure and the restriction to fixed time steps. Using Single Step Houbolt the algorithm is computationally more convenient compared to the standard Houbolt method, but because of its damping properties, the time steps have to be chosen carefully [43]. The increment number was decreased from originally 5000 to 50 increments. Therefore three simulations were run, two using Houbolt (50 and 500 increments) and one using Newmark (1000 increments without damping). Fibre stress and matrix strain values were compared and a mean deviation of 1-2% was found from the model using 50 increment to the model using 1000 with deviation peaks rising up to 10 or 15%. A deviation of 2% is admissible. The peak deviations of 10 to 15% are high, but as every fibre value was averaged over 32 integration points (four per fibre layer over eight elements in z direction), the probability of a deviation of 10% or 15% decreases significantly.

5.4 Comparison and benchmarking

5.4.1 Fibre angles

The following orientations were found in the literature:

(a) $\alpha_0 = 32\,^\circ, \nabla_r\alpha = 0\,^\circ, \nabla_t\alpha = 0\,^\circ$[12, 22]

(b) $\alpha_0 = 28\,^\circ, \nabla_r\alpha = 17\,^\circ, \nabla_t\alpha = 0\,^\circ$[23]

(c) $\alpha_0 = 67.3\,^\circ, \nabla_r\alpha = 0\,^\circ, \nabla_t\alpha = -43.8\,^\circ$[24]

Moreover Zhu [25]who used a similar sectioning as in this study (five sections going from anterior to posterior) measured fibre angles over seventeen fibre

layer. The data was linearly interpolated over each section and finally for each of them a linear equation was presented. As the exact measured values were not mentioned and could not be obtained on enquiry, using the linear radial equations, the value of the extreme inner and outer layers were calculated. Positive and negative fibre layers were averaged and a plane was fitted to the data using the least squares method [5]. The result was the following:

- $\alpha_0 = 52.3\,^\circ, \nabla_r\alpha = 14.1\,^\circ, \nabla_t\alpha = -39.0\,^\circ$

Thus, Zhu's results practically unify both diverging propositions of either only a radial gradient or only a tangential gradient, which is quite remarkable. Still, Zhu compared them only to the results of Holzapfel [32] and concluded that, the dimension of the used specimen is smaller than in the study of Holzapfel and thus, it is more representative of the mechanical property and fibre orientation of each point [25]. Moreover Zhu found the lowest angles in the right lateral segment. First this suggests that specimens are not symmetrical and second, although this is only a speculation, could be induced by coupled flexion and torsion to the right, occurring more often than the same movement to the left[6].

The orientations which resulted out of the simulations were:

(a) $\alpha_0 = 32.2\,^\circ, \nabla_r\alpha = 0\,^\circ, \nabla_t\alpha = 0\,^\circ$ (flexion)

(b) $\alpha_0 = 52.5\,^\circ, \nabla_r\alpha = 0\,^\circ, \nabla_t\alpha = 0\,^\circ$ (extension)

[5] For the over-defined system $Ax = b$ the sum of the least square error $((b-Ax)^T(b-Ax))$ was minimized[34]. $Ax = b$ is equal to $\alpha_0 + \nabla_r\alpha * r_i + \nabla_t\alpha * t_i = \alpha_i$ and therefore $a_{i1} = 1$, a_{i2} and a_{i3} are the radial and tangential relative position of the measurement, b_i is the measurement value and x is the solution vector $[\alpha_0, \nabla_r\alpha, \nabla_t\alpha]$.

[6] As for the majority of populations left section of the brain is dominant, the probability that an individual looks back over the right shoulder is higher than the opposite

(c) $\alpha_0 = 64.5\,^\circ, \nabla_r\alpha = 10.3\,^\circ, \nabla_t\alpha = 0\,^\circ$ (compression)

(d) $\alpha_0 = -2.0\,^\circ, \nabla_r\alpha = 23.0\,^\circ, \nabla_t\alpha = 0\,^\circ$ (torsion)

Except torsion all of the encountered values are in the range of orientations found in the literature. The angle found under flexion is similar to those reported by Marchand, Ahmend and Galante[12, 22]. The result under compression is similar to the maximal angle measured by Eberlein[24]. Torsion and compression show a similar radial gradient to those found in literature. However, when put together, our current results can not explain the most recent results of Zhu, nor those of Cassidy[23] or Eberlein[24]. It should be highlighted that tangential gradients were never found, though such gradients were expected, at least under flexion and extension. More important is to mention that in the case of compression, a local FCQ maxima was found, which would support the FCQ result obtained from the semi-cylinder model.

The optimal fibre orientations were only in function of α_0 and can therefore only be compared to constant fibre orientations in the AF. However, time was short and the results presented before were obtained after 50 iterations only. When running optimizations on the simplified models, $\overline{FCQ}$ always converged firs in direction of α_0t, and then in direction of $\nabla_r\alpha$ and $\nabla_t\alpha$.

5.4.2 Algorithm

As presented in the state of the art, to our knowledge, the only groups having proposed collagen fibre orientation algorithms are Driessen et al. and Hariton et al.[28]. The difference between the FCQ evaluation function and the preferred fibre direction algorithm (Eq. 1)is that FCQ judges a global ori-

entation in function of fibre stress and matrix strain and the preferred fibre direction suggests a preferred direction for each element in function of either element strain (Driessen) or elements stress (Hariton). As the preferred fibre direction algorithm was made for remodelling, a way had to be found to compare them with the results of the FCQ function. Due to implementation reasons (on the Matlab level the local element's fibre orientation is unknown) the benchmarking was only done in function of α_0. To compare in each element preferred fibre direction vector $\vec{e_{p,i}}$ with the actual fibre orientation $\vec{f_i}$ ($f_1 = g(\alpha)$ and $f_2 = g(-\alpha)$) over all elements, the following sum of dot products was calculated: $\sum_j min_j(\langle f_1, \vec{e_{p,1}}\rangle + \langle f_2, \vec{e_{p,2}}\rangle, \langle f_1, \vec{e_{p,2}}\rangle + \langle f_2, \vec{e_{p,1}}\rangle)$, which was stated to represent the correlation between actual fibre orientation, $\vec{f_i}$ and preferred fibre orientation, $\vec{e_{p,i}}$. Although around 0° degree the errors due to approximation of $vecf_i$ should be negligible. With increasing or decreasing fibre angle the accuracy fades, and comparisons were not representative any more.

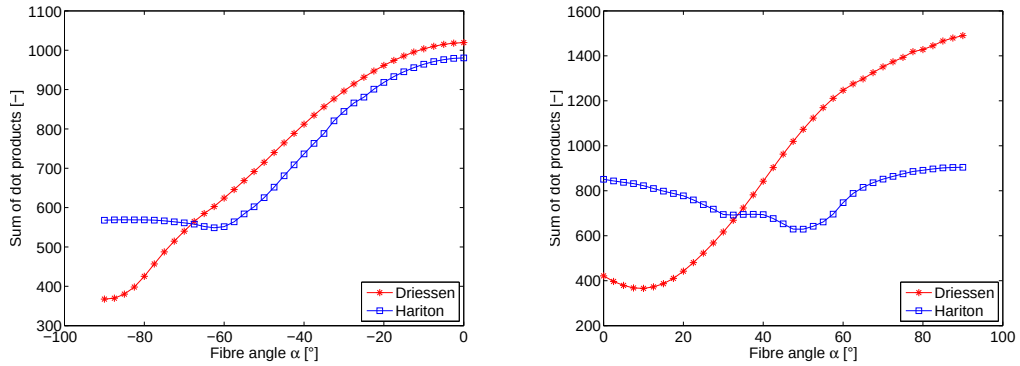

(a) Compression (b) Traction

Figure 25. Sum over all iteration points of the dot product between fibre vector and proposed fibre vector $\vec{e_{p,i}}$ (Eq. 1).

Under compression Driessen's algorithm could predict the expected optimal angle of $\pm 90^\circ$ (Fig. 25) and under traction, it gave an optimal fibre orientation of $\pm 12^\circ$. As matrix element's principal stresses (in the code fibre stress and matrix stress are separated) were used, the evaluation and the results of Hariton's algorithm are not meaningful. However, as principal strain and stress directions were the same Hariton's algorithm should lead to the same results as Driessen's algorithm. Comparing with the results of the current FCQ formulation Driessen obtain results, closer to the expected values. However, as Driessen's algorithm was written and tested in case of cartilage and arterial wall modelling, it it probable that it can explain a simple model like the semi-cylinder model under traction and compression. Yet, as Driessens formulation is close to the MSE formulation and close to the obtained results (Fig. 13), it should be emphasized that its performance in case of the AF first needed to be tested using the real lumbar spine model and is not expected to be strongly different to an formulation only using the MSE parameter.

5.5 Criticism and limitations

Probably, the main weakness of the study are the non anatomical fibre orientation which are allowed. In the nature a constant fibre orientation of 0° does not occur.

Also in terms of maximal stress or strains, some values were not realistic. For example, when the small model is under traction (10% deformation which is

realistic for the AF) and the fibre angle is set to 0 ° fibre stresses may rise up to 110 Mpa which is not a biologically relevant stress level. It could be argued that instead of using constant deformations, constant forces could be applied. Yet, if setting external stress to a constant value, at an optimal fibre orientation, strains also led to deformations that were bellow a realistic biological deformation. Also for the big model with constant biologically admissible fibre orientations and load, non-biological local fibre stresses were found (up to 350 Mpa!). It is difficult to say whether this may influence the RMS values which are in any case relative with a minimum of zero and a maximum of one. However, it shows some of the limitations of the implementation of the rebar formulation in Marc Mentat, respectively the "back-calculation" from an ordinary stress tensor to rebar stresses. Moreover, it has to be taken in account that wrong calculated stresses also could be due to a wrong implementation.

The limitations with respect to $\overline{FCQ}$ validation are mainly that it is difficult to verify what is really the "best" fibre orientation under a given load. For example under pure traction it is almost evident that the best fibre orientation is aligned with the principal strain/stress direction. But what happens if beside the traction a lateral load is applied? Cells may prefer a crossed collagen orientation which will give more lateral stability or a different orientation better adapted to obtain oxygen.

If taking into account matrix strain and fibre stress, which was the case in this study, how should they be weighted? It is possible that for a cell in the matrix a MSE value is more important then an RMS value.

Finally, there are several parameters and properties which was not accounted

for in our model. The effect of water in the AF, its visco-elasticity or non-symmetric geometry (in respect to the sagital plane) could be mentioned. Moreover, it was found that interlamellar connections [39, 40], which were not modelled, may involve greater numbers of molecular interactions than previously thought.

5.6 Pre-stress

As discussed previously, the radial stress distribution found under compression in the semi-cylinder model shows low or even no fibre stress in the outer part of the AF. Also for the real L4-L5 model the same behaviour was observed (e.g. under flexion ⇒ anterior AF is compressed ⇒ outer fibres are more stressed - Appendix A.0.4). Comparing this results to the aorta, zero fibre stresses (which is the aorta model are equal to negative stresses) or lower stresses in the outer annulus could indicate that it should be pre-stressed (Fig. 26). The fact that there is a constant internal pressure in the AF, which is 15 times higher than in the aorta underlines this fact. Pre-stress in the aorta is assumed to be only due to geometry. It has to be considered that in case of the AF it is probably more complicated because not only geometry dependant pre-stress could intervene but also pre-stress due to swelling. To our knowledge no experimental quantitative studies were reported about pre-stressed conditions in the AF fibres. Yet, if it is really pre-stressed this would completely change the whole concept of evaluation optimal fibre distributions in the AF fibre orientations and probably also of FE AF fibre modelling itself.

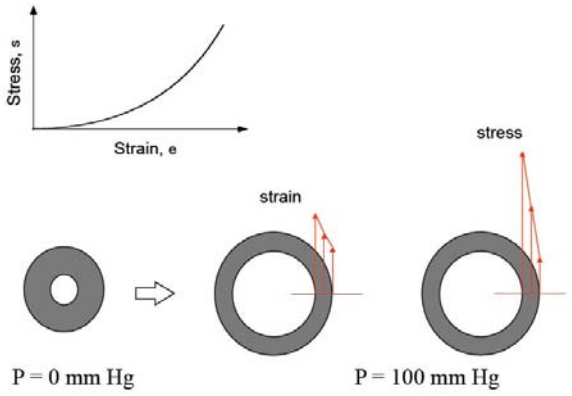

Figure 26. Stress and strain in absence of pre-stress in the case of the aorta (100mmHg = 13.3 kPa). Ordinarily under loaded conditions the stress distribution in the aorta is constant. Adapted from [41].

5.7 Optimization vs. remodelling

The logic deduction of the previous findings is to contrast optimization and remodelling. They are almost the same: Seeking the optimal properties in function of loads or other parameters. So what is the difference between remodelling and a structural optimization?

Remodelling, for example in case of a bone, changes the local element property using local information. The element does not know directly, what happens in remote elements and information is transmitted only by the neighbour elements. The evolution of element i is described by $\phi_{new,i} = f(\psi_{i,k})$ where $\phi_{new,i}$ is the new, adapted property and $\psi_{i,k}$ are k current or historical loadings, deformations or properties of element i [42]. A structural optimization procedure, in the way it was implemented, changes the local properties in function of global information. Elements receive direct information transmitted from some or all other elements through the implementation of a global objective function. Element's i evolution can be described as follow-

ing: $\phi_{new,i} = F(\psi_{i,k}, \sum_j^{N_k} \psi_{j,k})$ where $\phi_{new,i}$ is the new property, $\psi_{j,k}$ are k current or historical loadings, deformations or properties of any element j, N_k is a given number of element or their total number and F a function of N_k and k.

During remodelling, every single element will adapt to local "external" conditions. During a structural optimization, a single element does not a adapt, but the global structure of elements is adapted due to the global output. New properties are imposed from outside. This may be a disadvantage when exact local adaptation is more important and advantage when a global structure is required. Moreover, if the optimal position, composition, structure or result is a global trade-off between several parameters, it can probably only be achieved by an optimization procedure. At least it is difficult to imagine a reasonable solution if one element adapts to one condition and its neighbour to an other.

To link the comparison to other fields, at the level of information flow, an optimisation could be compared to swarm intelligence (bio-inspired artificial intelligence[7]) or wisdom of crowds (economics or sociology[8]) and remodelling as individual intelligence.

6 Conclusion

In general it can be concluded that a general computational framework to optimize annulus fibrosus (AF) orientations could be implemented and ver-

[7]One bird is unable to find food, where a swarm of birds using the information at every point of space "converges" faster to place where the food is situated.

[8]For example in case of Wikipedia the output of the crowd is higher than of the single individual.

ified. The necessary programs could be linked and their interaction work properly. Fibre orientation angle optimizations (50 iterations) were run on a complete L4-L5 model using the Fibre Contribution Quality (Eq. 3 to 8). The algorithm converged in all tested cases (flexion, extension, compression and torsion) and constant fibre angles between 32 and 68 and radial gradients between 10 and 17 degree were found. They could partly be compared with the literature, but finally it has to be concluded that due to local maxima and the FCQ function, which was not correct at the time the results are not valid.

A critical fibre angle of $\sim 56.6\,^{\circ}$ (traction) and $\sim 33.4\,^{\circ}$ (compression) was discovered. Over this angle under uni-axial compression or bellow this angle traction fibres are not stressed any more.

A one element structure is insufficient in terms of convergence.The Houbolt discretisation using 50 iterations showed an average error of $\sim$ 1-2% and peak deviation of 10 to 15%. Due to the averaging, over 32 nodes it was assumed that it does not affect the results significantly.

However, with respect to convergence, biological imitation or the validation procedure, the non-linearity of the AF tissue, its fibres and ground substance, still leads to challenging and complicated solutions. The evaluation of the $\overline{FCQ}$ function turned out to be more complex as expected. At many steps of the work, new issues arose and had to be handled or taken into consideration. Values needed to be averaged, singularity avoided and accuracy had to be increased while keeping reasonable computational cost. Several different $\overline{FCQ}$ versions could be assessed using the semi-cylinder model. The $\overline{FCQ}$ function turn out to be valid, when using it without its $\overline{RSD}$ parameter.

In Any case this can be justified by the use of the $\overline{MSE}$ parameter, which somehow is also a uniformity measurement of stress or strain distribution. For more complex problems the use of an algorithm taking into account fibre stress and matrix shear strain only should be further explored. Also the version using the variance of the radial stress distribution shall be further assessed.

Optimization can be compared to modelling remodelling. It is proposed according to the required information flow one maybe more suitable than the other: Remodelling in case of one single local parameter to optimize and optimization in case of several local parameters influenced by global variables or constraints.

Using Zhu's data it was possible to solve one of the main issues of collagen fibre orientations in the AF and to bring together the two hypotheses of either only radial or only tangential fibre orientation gradient. The orientation found was $\alpha_0 = 52.3\,^\circ, \nabla_r\alpha = 14.1\,^\circ, \nabla_t\alpha = -39.0\,^\circ$.

Pre-stress is an important and non-negligible factor. Under the assumption an optimal stress distribution in the AF is uniform, they have to be implemented as initial conditions in the finite element models.

6.1 Recommendations

- Currently optimization dimensions are α_0, $\nabla_r\alpha$ and $\nabla_r\alpha$. As most optimisation only converged in the direction of α, it is recommended to

change the position of α_0 from the outer anterior AF to the middle of the domain (between middle(1) and middle(2) respectively lateral and posteo-lateral segment). Moreover it is necessary to run optimisation with more than 50 iterations.

- Run optimizations using $\overline{FCQ} = f(\overline{RMS}, \overline{MSE})$
- Non-biological fibre stress output (Fig. 22) have to be addressed and the used implementations further validated.
- As there is at least one multilamellar bridge per 20 ° anterior segment[40] (and probably also other segments), their influence should be evaluated in the $\overline{FCQ}$ function.
- Then AF model fibres should be pre-stressed.

6.1.1 Technical recommendations

Most of the technically important aspects are mentioned in section 3.3. Moreover, every section of new code is commented. Still, for some of the coding it may take some time to understand how things were exactly implemented. Marc Mentat 2005 and 2007 are not totally compatible. Thus, it is **strongly** recommended to erase all materials in the model, renew and re-attribute them, when passing form one version to the other. Errors may arise at a very late state and take a long time to localize. Do not duplicate material properties. Be aware of irregularities, which may be induced by duplicating elements.

7 Acknowledgement

Jérôme: Gracias por todo lo has hecho por mi. Tu cotidiana ayuda, tus conocimientos y tu profesionalidad contribuyeron en gran medida al resultado final de este trabajo. Tu consistencia y paciencia me enseñaron tantas cosas,que pueden ser mucho mas de lo que piensas.

I would like to thank my supervisors Damien Lacroix and Dominque Pioletti. I learned a lot during this semester, whether is was in respect to bio-mechanics, personal relationships or communication. Thank you for organising and supervising my master thesis. Moreover, Andrea, Andy, Cécile, Clara, Sara y Martin: It was a pleasure to work together with you. Thank you for your help and your inputs.

Karolin, muchas gracias por haber estado junto a mi y por todas las cosas lindas que pasamos durante este tiempo en Barcelona. Lisa, Felipe y Stefan: Fue un placer vivir con ustedes.

8 Bibliography

References

[1] Shankar H., MBBS, Scarletta J. A., Abram S. E., *Anatomy and pathophysiology of intervertebral disc disease.* Techniques in Regional Anesthesia and Pain Management 13:67-75, 2009

[2] Noailly J., Wilke H. J., Planella J. A, Lacroixa D., *How does the geometry affect the internal biomechanics of a lumbar spine bi-segment finite*

element model? Consequences on the validation process. J. Biomechanics, 40:2414-25, 2007

[3] *Low Back Pain Fact Sheet.* Office of Communications and Public Liaison, National Institute of Neurological Disorders and Stroke, National Institutes of Health, Bethesda, MD 20892, NIH Publication No. 03-5161, 2003
*http : //www.ninds.nih.gov/disorders/backpain/detail*ь*ackpain.htm*

[4] OpDeBeek R., Hermans V. *Research on work-related low back disorders.* European Agency for Safety and Health at Work, Office for Official Publications of the European Communities, Luxembourg, 2000

[5] van Zundert J., van Kleef M., *Low Back Pain: From Algorithm to Cost-Effectiveness?* World Institute of Pain, Pain Practice, Volume 5, Issue 3:179Ű189, 2005

[6] Ehrlich G. E., *Low Back Pain.* Bulletin of the World Health Organization 81(9), 2003

[7] Pope M. H., Wilder D. G., Krag M. H., *Biomechanics in the lumbar spine - Basic principles. In the adult spine. Principles and practice.* Edited by Frymoyer J. W., Drucker T. B., Hadler N. M., Kostuik J. P., Weinstein J. N., Whitecloud T. S., pp:1487-1504, Raven Press, New York

[8] Comin M et al., *Biomécanica del raquis y sistemas de reparación.* Instituto de Biomécanica de Valencia, Valencia

[9] binx101.wordpress.com

[10] eOrthopod, Medical Multimedia Group, LLC, 2009 www.eorthopod.com

[11] Heuer F., Schmidt H., Wilke H. J., *The relation between intervertebral disc bulging and annular fiber associated strains for simple and complex loading.* Journal of Biomechanics, 41:1086-1094, 2007

[12] Marchand F., Ahmed A. M., *Investigation of the laminate structure of lumbar disc annulus fibrosus.* Spine 15:402-410, 1990

[13] Humzah M. D., Soames R. W., *Human intervertebral disc: Structure and function.* The Anatomical Record 220:33-356, 1988

[14] Guerin H. A. L., Elliot D. M., *Degeneration affects the fibre reorientation of human annulus fibrosus under tensile load.* Journal of Biomechanics 39:1410-1418, 2006

[15] Eberlein R., Holzapfel G. A., Schulze-Bauer C. A. *An anisotropic model for annulus tissue and enhanced finite element analyses of intact lumbar disc bodies.* Computer Methods in Biomechanics and Biomedical Engineering 00:1-20

[16] Shirazi-Adl S. A., Shrivastava S. C., Ahmed A. M., *Stress analysis of the lumbar disc-body unit in compression. A threedimensional nonlinear finite element study.* Spine 9:120-134, 1984

[17] Spilker R. L., Jakobs D. M., Schult, A. B., *Material constants for a finite element model of the intervertebral disk with a fiber composite annulus.* Journal of Biomechanical Engineering 108:1-11, 1986

[18] Yin L., Elliott D. M. , *A biphasic and transversely isotropic mechanical model for tendon: application to mouse ail fascicles in uniaxial tension.* Journal of Biomechanics 37:907-916, 2004

[19] Heather A. L. G., Dawn M. E., *Degeneration affects the fiber reorientation of human annulus fibrosus under tensile load .* Journal of Biomechanics, 39:1410-1418, 2006

[20] Bogduk N., *Clinical anatomy of the lumbar spine and sacrum.* Churchill Livingstone, Edinburgh, London, New York, Oxford, Philadelphia, St Louis, Sydney, Toronto, 1997

[21] Ralphs J., *Cellular control of extracellular matrix secretion and organisation in connective tissues.* School of Biosciences, Cardiff University, Cardiff, Wales, UK, 2003-09
http://www.cardiff.ac.uk/biosi/contactsandpeople/stafflist/q-t/ralphs-jim-dr.html

[22] Galante J.O, *Tensile properties of the human lumbar annulus fibrosus.* Orthopaedica Scandinavica, 100:1-91, 1967

[23] Cassidy J. J., Hiltner A., Baer E., *Hierarchical structure of the intervertebral disc.* Connective Tissue Research 23:75-88, 1989

[24] Eberlein R., Holzapfel G. A., Schultze-Bauer C. A. J., *An anisotropic constitutive model for annulus tissue and enhanced finite element analysis of intact lumbar disc bodies.* Computer Methods in Biomechanics and Biomedical Engineering, 4:209-230, 2001

[25] Zhu D., Gua G., Wub W., Gong H., Zhu W., Jiang T., Cao Z., *Microstructure and mechanical properties of annulus fibrous of the L4-5 and L5-S1 intervertebral discs.* Clinical Biomechanics, 23:74-82, 2008

[26] Driessen N .J. B. et al, *A computational model for collagen fibre remodelling in the arterial wall.* Journal of Theoretical Biology 226:53-64, 2004

[27] W. Wilson et al., *Prediction of collagen orientation in articular cartilage by a collagen remodelling algorithm.* OsteoArthritis and Cartilage 14:1196-1202, (2006)

[28] Baaijens F., Bouten C., Driessen N., *Modeling collagen remodeling.* Journal of Biomechanics, Article in Press,doi: 10.1016/ j.jbiomech .2009.09.022, 2009

[29] Hariton I., deBotton G., Gasser T. C., Holzapfel G. A. *Stress-driven collagen fiber remodeling in arterial walls.* Biomechanics and Modelling in Mechanobiology, 6(3):163-175, 2007

[30] Noailly J., Planell J. A., Lacroix D., *On the collagen criss-criss angles in the annuli fibrosi of lumbar spine finite element models.* Article in press, Biomechanics and Modelling in Mechanobiology

[31] Driessen N. J. B., Wilson W., Bouten C. V. C., Baaijens F.P.T., *A computational model for collagen fibre remodelling in the arterial wall.* Journal of Biomech. 36:1151-58,2003

[32] Holzapfel G. A., Schulze-Bauer C. A., Feigl G., Regitnig P., *Single lamellar mechanics of the human lumbar annulus fibrosus.* Biomechanics Modelling Mechanobiology, 3:125-140, 2005

[33] Iatridis J.C., Gwynn I., *Mechanisms for mechanical damage in the intervertebral disc annulus fibrosus.* Journal Of Biomechanics 37:1165Ű1175, 2004

[34] *Matlab© R2009a help manual.* MathWorks Inc., 2009

[35] Lewis R. M., Torczon V., Trosset M. W. *Direct Search Methods: Then and Now.* Institute for Computer Applications in Science and Engineering, NASA Langley Research Center, Hampton, ICASE Report No. 26, 2000

[36] Medscape,WebMD, LLC, 101 Eight Avenue, Suite 700, New York, NY 10011, 2009 www.medscape.com

[37] Floreano D. and Mattiussi C., *Bio-inspired Artificial Intelligence.* Cambridge MA, MIT Press, 2008

[38] Jones A. C. , Wilcox R. K., *Finite element analysis of the spine: Towards a framework of verification, validation and sensitivity analysis.* Medical Engineering & Physics, 30:1287-1304, 2008

[39] Michalek A. J., Buckley M. R., Bonassar L.J., Cohen I., Iatridis J. C., *Measurement of local strains in intervertebral disc anulus fibrosus tissue under dynamic shear: Contributions of matrix fiber orientation and elastin content.* Journal of Biomechanics, 42:2279-2285 (2009)

[40] Schollum M. L., Robertson P. A., Broom N. D., *Microstructure and mechanical disruption of the lumbar disc annulus.* Spine Volume 33, Number 25, 2702-2710, 2008

[41] Stergiopuols N., *Stress and strain in absence of pre-stress.* Cours slides, Biomécanique intégrative, Swiss Institute of Technology, Lausanne, 2009

[42] Pioletti D., *Bone remodelling.* Cours slides, Biomécanique du système musculo-squelettique, Swiss Institute of Technology, Lausanne, 2008

[43] *MSC. Marc© Volume A: Theory and User Information.* MSC. Software Corporation, 2 MacArthur Place Santa Ana, CA 92707

[44] Noailly J., *Model developments for in silico studies of the lumbar spine biomechanics.* Doctoral thesis, (2009)

[45] Wesley A., *Anatomy and pathophysiology of intervertebral disc disease.* Massachusetts, 2nd Edition, 1994

[46] Meakin J. R. et al, *The effect of partial removal of the nucleus pulposus from the intervertebral disc on the response of the human annulus fibrosus to compression.* Clinical Biomechanics, 16:121-128, 2001

[47] Buckwalter J. A., *Aging and degeneration of the humanintervertebral disc.* Spine 20:1307-1314, 1995

A Appendix - Complementary results

A.0.2 GA

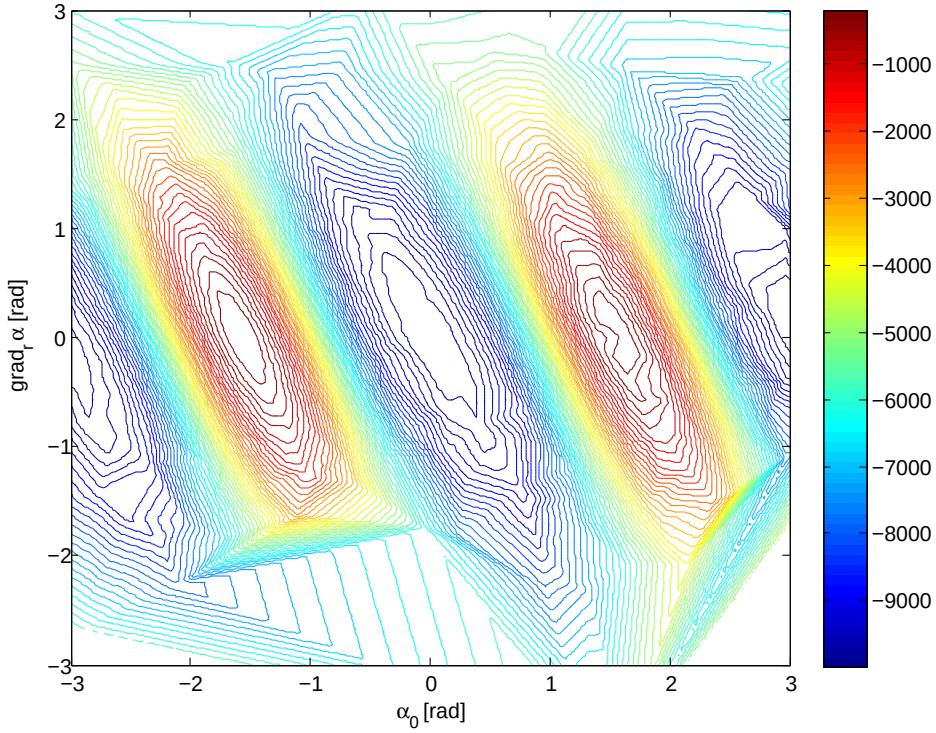

Figure 27. Interpolation of all solutions exploration by a genetic algorithm - crossover fraction: 0.8, population size: 80, generations: 90, Elitism: One individual. On a strongly simplified geometry the algorithm converged (FCQ tolerance of $< 10^6$) the 4321 FCQ function evaluations. Interpolating a hyper-surfaces the result was used to get an idea of the initial solution space. The figure represents FCQ values varying in function of $alpha_0$ and $\nabla_r \alpha$. At that time the algorithm was still strongly underdeveloped.

A.0.3 MSE

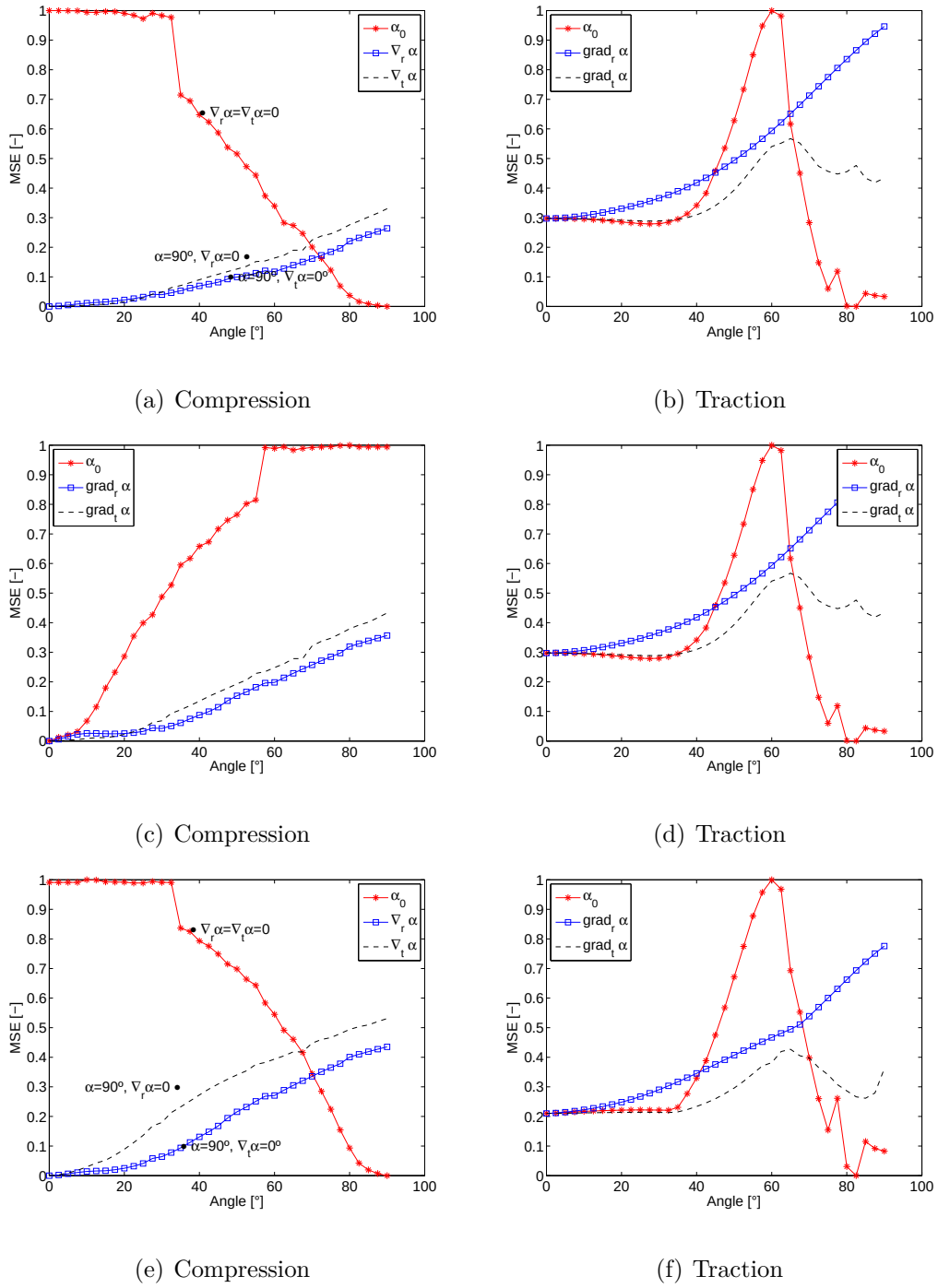

(a) Compression (b) Traction

(c) Compression (d) Traction

(e) Compression (f) Traction

Figure 28. MSE benchmarking. Deviation form optimal position in directions α_0, $\nabla_r\alpha$ and $\nabla_t\alpha$. a) and b): Final MSE (Eq. 6) c) and d): $MSE = \sum|\varepsilon_{ij}|, i \neq j$ e) and f) $MSE = \sum|\varepsilon_{13}|$.

A.0.4 Flexion

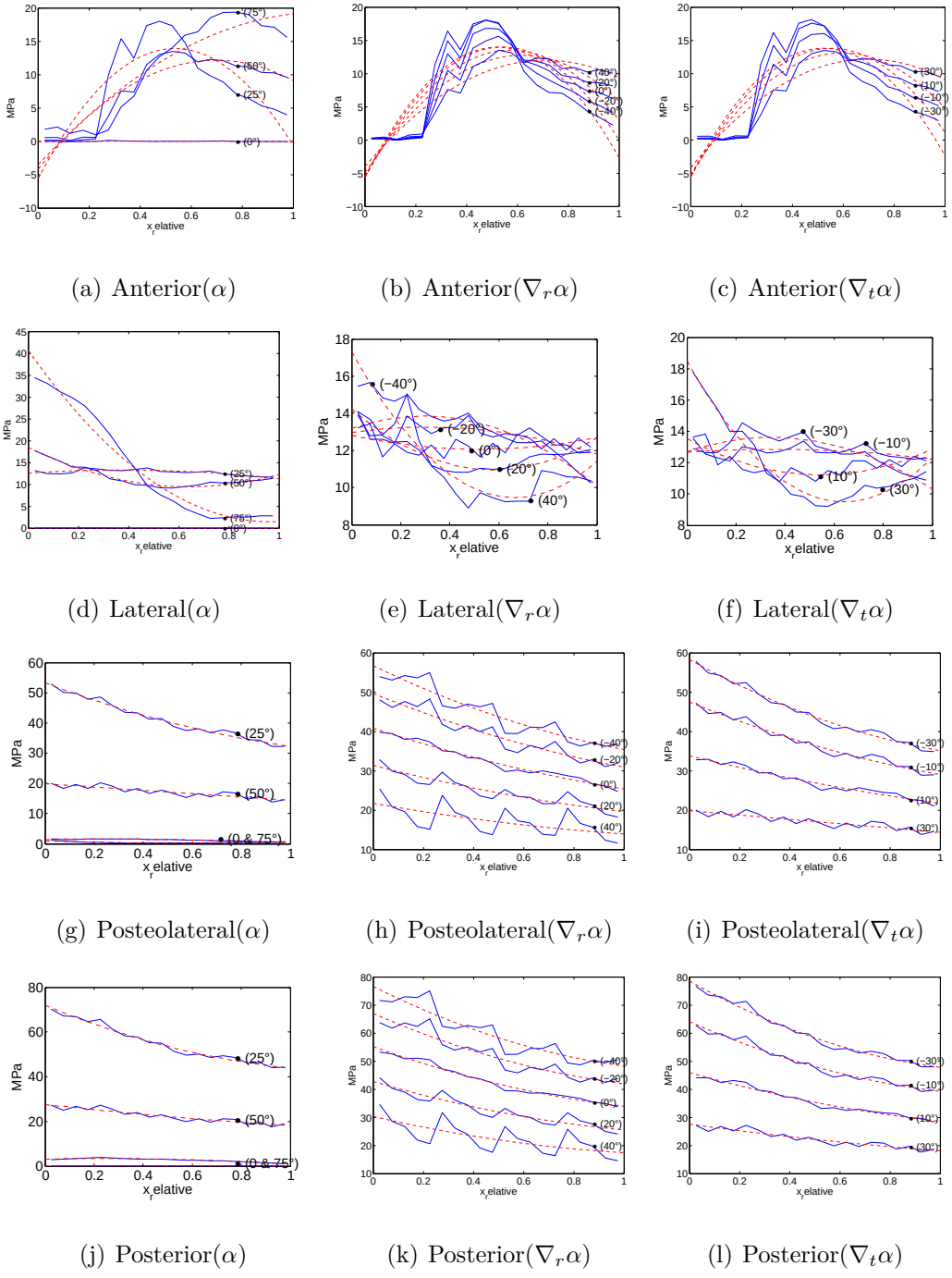

(a) Anterior(α) (b) Anterior($\nabla_r\alpha$) (c) Anterior($\nabla_t\alpha$)

(d) Lateral(α) (e) Lateral($\nabla_r\alpha$) (f) Lateral($\nabla_t\alpha$)

(g) Posteolateral(α) (h) Posteolateral($\nabla_r\alpha$) (i) Posteolateral($\nabla_t\alpha$)

(j) Posterior(α) (k) Posterior($\nabla_r\alpha$) (l) Posterior($\nabla_t\alpha$)

Figure 29. Example of all stress distributions in the AF under flexion. In case of $\nabla_r\alpha$ and $\nabla_t\alpha$ α_0 was kept at 35 ° and the gradients were changed around it.

B Matlab coding

The essential M-files are:

(a) Run_file

(b) Opti_fmin

(c) F_eval

(d) FCQ_eval

These files are presented bellow in there shortest version. The rest of the files, plotting, GA, ets. won't be presented in the report.

B.1 Run_file

```
% Reset maximal and minimal value
if 0==0
RMS_max=0;
RSD_max=0;
MSE_max=0;
save('FCQ_max_file','RMS_max','RSD_max','MSE_max')
RMS_min=10000;
RSD_min=1000;
MSE_min=1000;
save('FCQ_min_file','RMS_min','RSD_min','MSE_min')
end

% Evluate points / run iterations around alpha0 = 90  and grad_r = 0
```

```
14 iter=[];
15 iter_FCQ.val=[];
16 iter_FCQ.max=[];
17 iter_FCQ.min=[];
18 iter_FCQ.par=[];
19 save iter_file iter
20 save iter_FCQ_file iter_FCQ
21
22 for i=-90:5:90
23     for j=-90:5:90
24         F_eval([i+90-j/2,j,0]);
25     end
26 end
27
28 % Run an optimization - optimisation name, inital value, number of maximal
29 % function evaluation, continue old iteration? (leave it 0), run
30 % optimisations for minima or maxima (leave it 0.5), chose optimisation
31 % parameter 0=FCQ
32 opti_fmin_big('The_Queens_royal_FCQ_optimisation',[33,10,-35],100,1,0.5,0)
33
34 load iter_file
35 load iter_FCQ_file
```

B.2 Opti_fmin

```
1 function [history]=opti_fmin(optimization_name,
2    ...Input,max_fun_eval,i_continue, calc_init,opti_parameter)
3
4 % Inital values
```

```
5  if i_continue==0
6      alpha_0 = 35;
7      grad_alpha_r = 10;
8      grad_alpha_t = 10;
9  else %conintue using a previous calculated input value
10     alpha_0 = Input(size(Input,1),1);
11     grad_alpha_r = Input(size(Input,1),2);
12     grad_alpha_t = Input(size(Input,1),3);
13 end
14
15 % Constants (case, geometry & load specific variables)
16 n_r=4;
17 n_t=4;
18 n_m=3;
19
20 % M defines the "dimensions" of the output of a Marc Mentat simulation.
21 % The values of M must be entered maually. The material number is saved
22 % in M(i,1), the lines per block (see F_eval) in M(i,2),the number of tensor
23 % lines (see F_eval) inM(i,3) and the number of elements in the material
24 % (in the set) in M(i,4).
25 M = [17 13 6 160
26     18 13 6 320
27     19 13 6 160
28     1 3 1 48
29     2 3 1 48
30     3 3 1 48
31     4 3 1 48
32     5 3 1 48
33     6 3 1 48
34     7 3 1 48
```

```
35      8 3 1 48
36      9 3 1 32
37      10 3 1 32
38      11 3 1 32
39      12 3 1 32
40      13 3 1 32
41      14 3 1 32
42      15 3 1 32
43      16 3 1 32
44      ];
45
46  subroutine_name = ['subroutine_big_45'];
47  M_M_name = ['14_15_new_ROTATION_R_15.0'];
48  save('input_file','n_r','n_t','n_m','M','M_M_name',
49      ...'subroutine_name','opti_parameter')
50
51  % Matrix initalization
52  iter=[];
53  iter_FCQ.val=[];
54  iter_FCQ.max=[];
55  iter_FCQ.min=[];
56  iter_FCQ.par=[];
57  save iter_file iter
58  save iter_FCQ_file iter_FCQ
59  history.x = [];
60  history.fval = [];
61
62  % Calculate maximal values for MSE RSD and RMS
63  if calc_init == 1;
64      F_eval_inital;
```

```
65 elseif calc_init == 0;
66     RMS_max=0;
67     RSD_max=0;
68     MSE_max=0;
69     save('FCQ_max_file','RMS_max','RSD_max','MSE_max')
70     RMS_min=100000;
71     RSD_min=1000;
72     MSE_min=1000;
73     save('FCQ_min_file','RMS_min','RSD_min','MSE_min')
74 else
75     %use the existent values in the max & min file
76 end
77
78 % Calling the optimization function
79 options = optimset('outputfcn',@outfun,'TolX',1e-6,
80      ...'MaxFunEvals',max_fun_eval,'Display','iter');
81 [x,fval,exitflag,output] = fminsearch(@F_eval,
82      ...[alpha_0,grad_alpha_r,grad_alpha_t],options)
83
84 load iter_file iter
85 load iter_FCQ_file iter_FCQ
86
87 % Plot the results
88 % ...
89 %
90
91 % Save the the created optimization and data & files
92 dos(['md ',optimization_name]);
93 dos(['copy output_file.mat H:\Proyectistas\Andreas
94    ...\Run11_tors\',optimization_name,' /y ']);
```

```
95 % ...
96 %
97
98 % Internal function used during the iteration to write down the
99 % historical evolution of the algorithm
100 function stop = outfun(x,optimValues,state)
101      stop = false;
102      switch state
103          case 'init'
104              hold on
105          case 'iter'
106          % Concatenate current point and objective function
107            history.fval = [history.fval; optimValues.fval];
108            history.x = [history.x; x];
109          case 'done'
110              hold off
111          otherwise
112      end
113 end
114
115 end
```

B.3 F_eval

```
1 function F=F_eval(a);%(alpha_0,grad_alpha_r);%
2 tic
3 alpha_0=a(1);
4 grad_alpha_r=a(2);
5 grad_alpha_t=a(3);
```

```
6
7  load input_file M_M_name
8
9  tensor_name = ['Tensors (',M_M_name,') ['...
10     ,sprintf('%d',alpha_0),'_'...
11     ,sprintf('%d',grad_alpha_r),'_'...
12     ,sprintf('%d',grad_alpha_t),'].mat'];
13
14 % Check wheater this loadcase already exists
15 if exist(tensor_name,'file') == 0
16     % Save the values for the Marc Mentat simulation in a file
17     simu_file = fopen('COMMON_VAR', 'w');
18     fprintf(simu_file, '\t alpha_0 = %8.10f \n \t grad_alpha_r =
19               ...%8.10f \n \t grad_alpha_t =  %8.10f \n',
20               ...[alpha_0*pi/180,grad_alpha_r*pi/180,grad_alpha_t*pi/180]);
21     fclose(simu_file);
22
23     % Sall Marc Mentat which will access to the file saved previously
24     load input_file M_M_name subroutine_name
25     dos(['run_marc -j ',M_M_name,' -u ',subroutine_name,' -v no']);
26
27     %*************************************************************************
28     % The simulation (Marc Mentat) is finished - Read in the results.
29     %
30     % C_in contains the values calculated by Marc Mentat is a matrix of the
31     % following type:
32     %
33     % 314   2   5       |header                |
34     % 0.0012                    |              |
35     % 0.015                     |one tensor    |
```

```
36      % 0.0065                    |               |one block
37      % 23.25                                     |
38      % 85.25                                     |
39      % 31.45                                     |
40      %       .  (next block)
41      %       .
42      %
43      % Remark: No strings are allowed in the header.
44      %
45      % Stress(i,j,k) and Strain(i,j,k) contain stress and strain information of
46      % all elements of one simulation. i is the integration point number, j the
47      % tensor value (e.g j=1 == C11, j=2 == C22 or j=4 == C12, j=5 == C23, etc)
48      % and k the material.
49      %
50      % M defines the "dimensions" of the output of a Marc Mentat simulation. The
51      % values of M must be entered maually. The material number is saved in
52      % M(i,1), the lines per block in M(i,2),the number of tensor lines in
53      % M(i,3) (e.g for the example above M(i,2)=7 and M(i,3)=3) and the number
54      % of elements in the materias (in the set) in M(i,4).
55      %*************************************************************************
56      load input_file M
57
58      Strain=zeros(1,1,1);
59      Stress=zeros(1,1,1);
60
61      for k=1:size(M,1)
62          lines_per_block=M(k,2);
63          lines_per_tensor=M(k,3);
64          C_in = dlmread(['simu_results_' sprintf('%d',M(k,1)) '.txt']);
65          for i=1:lines_per_block:size(C_in,1)
```

```
66              for j=1:lines_per_tensor
67                  Strain((i-1)/lines_per_block+1,j,k) = C_in(i+j,1);
68                  Stress((i-1)/lines_per_block+1,j,k) = C_in(i+j+lines_per_tensor,1);
69              end
70          end
71      end
72      save(tensor_name,'Strain','Stress')
73  else
74      load(tensor_name, 'Stress', 'Strain')
75  end
76
77  % Evaluate the quality of the Simulation by calculating a objective or
78  % fitness function. Write the output F.
79  F=FCQ_eval(Strain,Stress);
80
81  % Save ther relevant values in a file
82  load iter_file iter
83  t=toc;
84  iter=[iter;[alpha_0,grad_alpha_r,grad_alpha_t,F,t]];
85  save iter_file iter
86
87  % Write the current state of the optimization to the command window
88  [alpha_0,grad_alpha_r,grad_alpha_t,F];
89  n = size(iter,1);
90  end
```

B.4 FCQ_eval

```
1  function F=FCQ_eval(Strain,Stress)
```

```
load input_file M n_r n_t n_m opti_parameter
load FCQ_max_file RMS_max RSD_max MSE_max
load FCQ_min_file RMS_min RSD_min MSE_min
load angle a
%************************************************************************
% FCQ returns the value of the objective function FCQ
%
% Input:
% Stress(i,j,k) and Strain(i,j,k) contain stress and strain information of
% all elements of one simulation. i the integration point number, j the
% tensor value (e.g j=1 == C11, j=2 == C22 or j=4 == C12, j=5 == C13, etc)
% and k the material.
%************************************************************************

%Inizialisation
FCQ_1 = 0;
FCQ_2 = 0;
MSE = 0;
s_31=0;
RSD = 0;
RMS = 0;
RMS_Q = zeros(size(Strain,3),5);

% Iterate over all fibre materials, n_m: # of matrix materials, n_t: # of
% tangential subsection, n_r: # number of radial subsections, a: current
% angle alpha
for k=n_m+1:size(Strain,3)
    for i=1:20*M(k,4)
        % Calculate RMS
        RMS=RMS+Stress(i,1,k)/(M(k,4)*20);
```

```
32      end
33      % Every fibre element consist of 20 integration points, iterate over all
34      % elements
35      for i=1:20:20*M(k,4)
36          % Five layer
37          for j=0:4:19
38              % In each layer four integration point
39              for n=0:3
40                  % Creat a matrix RMS_Q(q,p) where q is one material and p
41                  % the layer number
42                  RMS_Q(k-n_m,j/4+1)=RMS_Q(k-n_m,j/4+1)+Stress(i+j+n,1,k)/(M(k,4)*5);
43              end
44          end
45      end
46  end
47
48  %Iterate over all ground substance materials
49  for k=1:n_m
50      for i=1:size(Strain,1);
51          for j=4:6
52              % Sum over all shear strain components
53  %           MSE=MSE+abs(Strain(i,j,1));
54          end
55          % Calculate eigenvalues, principal strain directions, MSE and eigen
56          % vectors
57          lamba=eig([Strain(i,1,k) Strain(i,4,k) Strain(i,6,k);
58              Strain(i,4,k) Strain(i,2,k) Strain(i,5,k);
59              Strain(i,6,k) Strain(i,5,k) Strain(i,3,k)]);
60          MSE=MSE+abs((lamba(1)-lamba(3))/2)/M(k,4);
61          [V,D]=eig([Strain(i,1,k) Strain(i,4,k) Strain(i,6,k);
```

```
62              Strain(i,4,k) Strain(i,2,k) Strain(i,5,k);
63              Strain(i,6,k) Strain(i,5,k) Strain(i,3,k)]);
64          V1=V*D;
65
66          % Driessen et al. -> equations in the repot
67          v3=V1(:,3);
68          v3=v3/norm(v3);
69          if lamba(2)>0
70              v2=V1(:,2);
71              v2=v2/norm(v2);
72          else
73              v2=[0;0;0];
74              lamba(2)=0;
75          end
76          % Preferd fibre direction
77          ep1=(lamba(3).*v3+lamba(2).*v2)/sqrt(lamba(3)^2+lamba(2)^2);
78          ep2=(lamba(3).*v3-lamba(2).*v2)/sqrt(lamba(3)^2+lamba(2)^2);
79          % Actual fibre direction
80          f1=sin(a(1)/180*pi)*[0;0;1]+cos(a(1)/180*pi)*[0;1;0];
81          f2=sin(a(1)/180*pi)*[0;0;1]-cos(a(1)/180*pi)*[0;1;0];
82          % Use the cos() of the two vector pairs, which are closer
83          Dris=Dris+min(abs(dot(ep1,f1))+abs(dot(ep2,f2)),abs(dot(ep1,f2))
84              ...+abs(dot(ep2,f1)));
85      end
86  end
87  % Calculate RSD
88  x=1/(2*n_r*5):1/(n_r*5):1;
89  % Iterate over tangential sections
90  for i=1:n_t
91      RMS_Qr=0;
```

```
92      y=[];
93      % Iterate over radial section
94      for j=1:n_r
95          % Iterate over the five layers
96          for k=1:5
97              % Place fibrestresses of each layer in a consecutive radial
98              % vector. Sum over each the radial section
99              y=[y,RMS_Q((i-1)*n_r+j,6-k)]; % inverting direction: 6-k = 5,4,3,2,1
100             RMS_Qr=RMS_Qr+RMS_Q((i-1)*n_r+j,6-k);
101         end
102     end
103     % Average the vector in respect to the subsection
104 %    y=y./(RMS_Qr+1);
105     % Fit a second order polynom to radial vector or calculate its variance
106     P(i,:) = polyfit(x,y,2);
107     VAR = var(y);
108     % Plot the stress distribution
109     if 0==1
110         figure(i+1000)
111         funcy_funcy = @(x) P(i,1)*x.^2+P(i,2)*x+P(i,3); %P(i,1)*x+P(i,2);
112         plot(x,y)
113         legend('stress');
114         hold on;
115         x1=0:0.02:1;
116         plot(x1,funcy_funcy(x1),'r'); hold on;
117         title_name=['Anterior     ';...
118                     'Lateral      ';...
119                     'Posteolateral';...
120                     'Posterior    ';];
121         title(title_name(i,:))
```

```
122         legend('original','interpolation'); hold on;
123         xlabel('x_relative');ylabel('MPa');
124         load i j
125         text(x(9),y(9),['\bullet (' sprintf('%d',(j-1)*15) ' )'])
126         if i==4
127         j=j+1;
128         end
129         save i j
130     end
131     % Calcualte the final value of RSD
132      RSD=RSD+sqrt(4*P(i,1)^2+P(i,2)^2);
133 %     RSD=RSD+abs(4*P(i,1)^2+P(i,2)^2)/(RMS_Qr+1);
134 %     RSD=RSD+VAR;
135 %     RSD=RSD+abs(4*P(i,1)^2+P(i,2)^2)*RMS_Qr;
136 end
137
138 % Reset maximal or minamal values if necessary
139 if RMS>RMS_max
140     RMS_max=RMS
141     save('FCQ_max_file','RMS_max','RSD_max','MSE_max')
142 end
143 if RSD>RSD_max
144     RSD_max=RSD
145     save('FCQ_max_file','RMS_max','RSD_max','MSE_max')
146 end
147 if MSE>MSE_max
148     MSE_max=MSE
149     save('FCQ_max_file','RMS_max','RSD_max','MSE_max')
150 end
151 if RMS<RMS_min
```

```
152     RMS_min=RMS
153     save('FCQ_min_file','RMS_min','RSD_min','MSE_min')
154 end
155 if RSD<RSD_min
156     RSD_min=RSD
157     save('FCQ_min_file','RMS_min','RSD_min','MSE_min')
158 end
159 if MSE<MSE_min
160     MSE_min=MSE
161     save('FCQ_min_file','RMS_min','RSD_min','MSE_min')
162 end
163 % Calculate FCQ
164 FCQ = -1/log(1+exp(1)-exp(-2))*log(1-exp(-2)+exp(...
165       (RMS-RMS_min)/(RMS_max-RMS_min)...
166     -(RSD-RSD_min)/(RSD_max-RSD_min)...
167     -(MSE-MSE_min)/(MSE_max-MSE_min))); % "-log(...)" will maximise
168                 %RMS and minimize MSE resp. RSD, "log(...)" the inverse
169 % Optimize in respect to ... -> normally case 0. Return the value.
170 switch opti_parameter
171     case 0
172         F=FCQ;
173     case 1 %maximize RSM
174         F = -RMS;
175     case 2 %minimize RSM
176         F = RMS;
177     case 3 %maximize RSD
178         F = -RSD;
179     case 4 %minimize RSD
180         F = RSD;
181     case 5 %maximize MSE
```

```
182         F = -MSE;
183     case 6 %minimize MSE
184         F = MSE;
185     case 7 %other case or variation
186         F = s_31;
187         FCQ_3 = [(RMS/RMS_max)^2;(MSE/MSE_max)^2];%lsqnonlin
188 end
189 % Write tracking files
190 load iter_FCQ_file iter_FCQ
191 iter_FCQ.val=[iter_FCQ.val;(RMS-RMS_min)/(RMS_max-RMS_min),
192                           ...(RSD-RSD_min)/(RSD_max-RSD_min),
193                           ...(MSE-MSE_min)/(MSE_max-MSE_min),
194                           ...RMS,RSD,MSE,FCQ];
195 iter_FCQ.max=[iter_FCQ.max;RMS_max,RSD_max,MSE_max];
196 iter_FCQ.min=[iter_FCQ.min;RMS_min,RSD_min,MSE_min];
197 iter_FCQ.par=[iter_FCQ.par;P(i,1),P(i,2),lamba(1),lamba(3)];
198 save iter_FCQ_file iter_FCQ
199 end
```

C Fortran subroutine

```
1 c The code was strongly shortened
2
3     Subroutine Hypela2(...)
4
5     if (mats.eq.49) then
6 c  set Property ...
7     endif
```

```
8
9       return
10      end
11
12
13  C* * * * * *
14  C       REBAR
15  C
16  C       Input:
17  C       N is the element number.
18  C       NN(1) is the integration point number.
19  C       NN(2) is the layer number.
20  C       NN(3) is the integration point number in this layer.
21  C       T,PR,TR,A are to be defined by the user.
22  C       Required Output:
23  C       T is the nominal size in thickness direction.
24  C       PR is the relative position of rebar layer with respect to T.
25  C       MSC.Marc uses the ratio PR/T to position the rebar layer in the
26  C       thickness direction.
27  C       TR is the equivalent thickness of rebar.
28  C       A is the direction cosines of the rebar.
29  C* * * * * *
30
31      SUBROUTINE REBAR (N,NN,T,PR,TR,A)
32
33  C*************************************************************************
34  C   Initaialization of the variables
35  C
36  C   The COMMOM_VAR file contains the values alpha_0, grad_alpha_r and
37  C   grad_alpha_t
```

```
C*********************************************************************

      DIMENSION A(3),NN(3),Coord_No(3,8),Disp_No(3,8),Lext(8),
     c e1(3),e2(3),e3(3),X(3),Y(3),Z(3),R(3,3),A_in(3), A_in_2(3),
     c Δ_r(4),Δ_t(4),R1(3,3)

      REAL *8 X_A,Y_A,Z_A,PI,alpha_0, grad_alpha_r, grad_alpha_t,
     c n_r, n_t, a_one

      Integer i_cross,i_direct,n_matus_re
      PI = 6*asin(0.5)

      INCLUDE 'H:\PROYECTISTAS\Andreas\Run11_tors\COMMON_VAR'

C*********************************************************************
C   Local Axis & Rotation Matrix
C
C   In this section the local axis of each element in global coordinates
C   is calculated. Then using this three vectros a the rotation matrix can
C   be set up to turn vectors from a global to a local coordinates system.
C
C   Where:
C   X, Y, Z are the axis vectors of the element
C   LEXT is the external node number
C   Coord_No is the array with the coordinates of the element's nodes
C   X_A, Y_A, Z_A are the norms of the axis vectors
C   R is rotation matrix (global to local coordinate system)
C*********************************************************************
c Coordinates
      ICOD = 0
```

```
68      DO i = 1,8
69      LEXT(i) = NODEXT(LM(i))
70      CALL NODVAR(ICOD,LEXT(i),Coord_No(:,i),NQNCOMP,NQDATATYPE)
71      CALL NODVAR(ICOD_D,LEXT(i),Disp_No(:,i),NQNCOMP,NQDATATYPE)
72          DO j=1,3
73          Coord_No(j,i)=Coord_No(j,i)+Disp_No(j,i)
74          ENDDO
75      ENDDO
76
77  c Calculate Axis, normalisation
78      DO i=1,3
79      X(i) = (Coord_No(i,5)+Coord_No(i,6)+Coord_No(i,7)+Coord_No(i,8))/4
80       c -(Coord_No(i,1)+Coord_No(i,2)+Coord_No(i,3)+Coord_No(i,4))/4
81      ENDDO
82
83      DO i=1,3
84      y(i) = (Coord_No(i,1)+Coord_No(i,2)+Coord_No(i,5)+Coord_No(i,6))/4
85       c -(Coord_No(i,3)+Coord_No(i,4)+Coord_No(i,7)+Coord_No(i,8))/4
86      ENDDO
87
88      DO i=1,3
89      Z(i) = (Coord_No(i,2)+Coord_No(i,3)+Coord_No(i,6)+Coord_No(i,7))/4
90       c -(Coord_No(i,1)+Coord_No(i,4)+Coord_No(i,5)+Coord_No(i,8))/4
91      ENDDO
92
93      X_A=ABS(sqrt(DOT_PRODUCT(X,X)))
94      Y_A=ABS(sqrt(DOT_PRODUCT(Y,Y)))
95      Z_A=ABS(sqrt(DOT_PRODUCT(Z,Z)))
96      DO i=1,3
97      X(i)=X(i)/X_A
```

```
98      Y(i)=Y(i)/Y_A
99      Z(i)=Z(i)/Z_A
100     ENDDO
101
102   c Correct wrong orientated element using Eularian rotations
103     R = RESHAPE( (/X(1),Y(1),Z(1),
104      c             X(2),Y(2),Z(2),
105      c             X(3),Y(3),Z(3) /), (/ 3, 3 /) )
106
107     if ((N.ge.4096).and.(N.le.4413)) then
108         a_one=1.0
109         R1 = RESHAPE( (/a_one,0,0,
110      c                0,cos(PI/2),-sin(PI/2),
111      c                0,sin(PI/2), cos(PI/2)/), (/ 3, 3 /) )
112
113     endif
114   C**********************************************************************
115   C   Fibre Distribution in the Annulus Fibrosus
116   C
117   C   Where:
118   C   n_r is the number of subdomains in the radial direction
119   C   n_t is the number of subdomains in the tangential direction
120   C   Δ_r/_t is a vector conating the ....
121   C   A_1, A_2, ... are the directive vectors of one rebar layer
122   C**********************************************************************
123
124     n_r=4
125     n_t=4
126     n_matus_re=0
127
```

```
128       do i = 1,n_r
129       Δ_r(i)=1-i/n_r
130       end do
131
132       do i = 1,n_t
133       Δ_t(i)=(i-1)/(n_t-1)
134       end do
135
136   c   ANT
137   c   ****
138       if (matus(2).eq.(1+n_matus_re)) then
139           d_r = Δ_r(4)
140           d_t = Δ_t(1)
141           i_dir_e = 1
142           TR = 0.211115026
143       else if (matus(2).eq.(2+n_matus_re)) then
144           d_r = Δ_r(3)
145           d_t = Δ_t(1)
146           i_dir_e = -1
147           TR = 0.277088472
148       else if (matus(2).eq.(3+n_matus_re)) then
149           d_r = Δ_r(2)
150           d_t = Δ_t(1)
151           i_dir_e = 1
152           TR = 0.277088472
153       else if (matus(2).eq.(4+n_matus_re)) then
154           d_r = Δ_r(1)
155           d_t = Δ_t(1)
156           i_dir_e = -1
157           TR = 0.356256607
```

```
158
159
160 c    LAT
161 c    ****
162      else if (matus(2).eq.(5+n_matus_re)) then
163          d_r = a_r(4)
164          d_t = a_t(2)
165          i_dir_e = 1
166          TR = 0.237504405
167      else if (matus(2).eq.(6+n_matus_re)) then
168          d_r = a_r(3)
169          d_t = a_t(2)
170          i_dir_e = -1
171          TR = 0.237504405
172      else if (matus(2).eq.(7+n_matus_re)) then
173          d_r = a_r(2)
174          d_t = a_t(2)
175          i_dir_e = 1
176          TR = 0.237504405
177 c        ...
178 c
179 c Always start with the outer anterior section.
180      endif
181
182 c Set layer properties
183      T = 1
184      if (NN(2).eq.1) then
185              PR = 0.1
186          i_dir=1
187      else if (NN(2).eq.2) then
```

```
188               PR = 0.3
189           i_dir=-1
190       else if (NN(2).eq.3) then
191               PR = 0.5
192           i_dir=1
193       else if (NN(2).eq.4) then
194               PR = 0.7
195           i_dir=-1
196       else if (NN(2).eq.5) then
197               PR = 0.9
198           i_dir=1
199       endif
200
201   c Orientate fibres
202       A_in(1)=0
203       A_in(2)=i_dir_e*i_dir*sin(alpha_0+grad_alpha_r*(d_r+PR/n_r)+
204        c grad_alpha_t*d_t)
205       A_in(3)=cos(alpha_0+grad_alpha_r*(d_r+PR/n_r)+grad_alpha_t*d_t)
206
207
208   C**********************************************************************
209   c    Output
210   c
211   c    Rotate the vector into the local coordinates system (element)
212   C**********************************************************************
213
214       A= MATMUL(A_in,R)
215       A=A/ABS(sqrt(DOT_PRODUCT(A,A)))
216
217       RETURN
```

```
218       END
219
220   C*********************************************************************
221   C
222   C   Write Output files
223   C
224   C*********************************************************************
225
226       SUBROUTINE ELEVAR(...)
227
228   c Decide when to write the ouput file!!!
229       if (inc.eq.48) then
230
231   c A Marix file
232       if (Matus(1).eq.17) then
233       open (unit=21,status='old',file='simu_results_17.txt',
234        c access='sequential')
235       WRITE(21,*) N1, NN1, KCUS1
236       do i = 1,6
237       WRITE(21,*) Gstran1(i)
238       enddo
239       do i = 11,16
240       WRITE(21,*) Gstres1(i)
241       enddo
242       endif
243
244   c A Rebar file
245       if (Matus(1).eq.9) then
246       open (unit=22,status='old',file='simu_results_9.txt',
247        c access='sequential')
```

```
248       WRITE(22,*) N1, NN1, KCUS1
249       WRITE(22,*) Gstran1
250       WRITE(22,*) Gstres1
251       endif
252
253       endif
254       RETURN
255       END
```